Document reference: IRM/GALOCAD/OUT220-1	Deliverable: OUT220-1	Date: 29-April-2008 Version: 2
Contract ref: GJU/06/2423/CTR/GALOCAD	Written by: R. Warnant, G. Wautelet, J. Spits, S. Lejeune	Verified by: R. Warnant

GALOCAD

Development of a Galileo Local Component for the nowcasting and forecasting of atmospheric disturbances affecting the integrity of high precision Galileo applications.

WP 220 Technical Report:

"Characterization of the ionospheric Small-scale activity"

Royal Meteorological Institute of Belgium, 3 Avenue Circulaire, B-1180 Brussels, Belgium.

LIST OF ABBREVIATIONS

BDN	Belgian Dense Network
GI/BAS	Geophysical Institute of the Bulgarian Academy of Sciences
GNSS	Global Navigation Satellite System
GPS	Global Positioning System
IMF	Interplanetary Magnetic Field
Kd	K index for Dourbes (Belgium)
NWP	Numerical Weather Prediction models
RINEX	Receiver Independent Exchange format
RMI	Royal Meteorological Institute
ROB	Royal Observatory of Belgium
RoTEC	Rate of TEC (TEC time derivative)
RTK	Real Time Kinematics
TEC	Total Electron Content
TECU	TEC Unit
TID	Travelling Ionospheric Disturbance
WP	Work Package

TABLE OF CONTENT

1. INTRODUCTION

The effect of the ionosphere on GNSS signals mainly depends on the Total Electron Content or TEC. The Total Electron Content is the integral of the ionosphere electron concentration on the receiver-to-satellite path. GNSS differential applications are based on the assumption that the measurements made by the reference station and by the mobile user are affected in the same way by the different error sources, in particular by the ionospheric effects. Therefore, these applications will not be affected by the absolute TEC but by gradients in TEC between the reference station and the user.

Small-scale structures in the ionosphere are the origin of gradients in TEC which can degrade the accuracy of differential applications even on distances of a few km. Such events could pose a threat for high accuracy GNSS applications. In this report, we characterize the different small-scale disturbances which can be encountered in a mid-latitude European station (Brussels, Belgium).

GNSS carrier phase measurements can be used to monitor local TEC variability. At any location, several GPS satellites can simultaneously be observed at different azimuths and elevations. Every satellite-to-receiver path allows to "scan" the ionosphere in a particular direction. The more satellites are simultaneously observed, the "denser" the information on the ionosphere is. In particular, smaller-scale ionospheric structures can be detected by monitoring TEC high frequency changes at a single station. Wanninger (1992) and Wanninger (1994) has developed a method allowing to monitor ionospheric irregularities based on a combination of GPS dual frequency phase measurements. In particular, this method was applied to scintillation monitoring in Brazil. Warnant (1996, 1998 and 2000) further developed the method for conducting "climatological" studies on smaller-scale ionospheric activity at the mid-latitude station in Brussels, Belgium.

2. DETECTION OF IONOSPHERIC SMALL-SCALE DISTURBANCES

2.1. Methodology

As already mentioned, TEC variability can be monitored using GNSS measurements (Warnant et al., 2000).
The simplified mathematical model of phase measurements made by receiver A on satellite i, $\varphi_{A,k}^{i}$ (in cycles) can be written as follows (Seeber (2003); Leick (2004)):

$$\varphi_{A,k}^{i} = \frac{f_k}{c}\left(D_A^i + T_A^i - I_{A,k}^i + c\left(\Delta t^i - \Delta t_A\right) + M_{A,k}^i \right) + N_{A,k}^i + \varepsilon_{A,k}^i \qquad (2.1)$$

with:

k , the carrier frequency (L1 or L2)

D_A^i, the geometric distance between receiver A and satellite i ;

$I_{A,k}^i$, the ionospheric error (m) on carrier *k*;

T_A^i , the tropospheric error (m);

Δt_A, the receiver clock error (the synchronisation error of the receiver time scale with respect to GPS time scale) ;

Δt^i, the satellite clock synchronisation error (the synchronisation error of the satellite time scale with respect to GPS time scale) ;

$N_{A,k}^i$, the phase ambiguity on carrier *k* (integer number) ;

$M_{A,k}^i$, multipath effect on carrier *k* ;

$\varepsilon_{A,k}^i$, noise on carrier *k* ;

f_k, the considered carrier frequency (L1 or L2).

If we neglected higher order terms (terms in f_k^{-3}, f_k^{-4} …), the ionospheric error $I_{A,k}^i$ is given by:

$$I_{A,k}^i = 40.3 \frac{TEC_A^i}{f_k^2} \tag{2.2}$$

with :

TEC_A^i, the slant TEC from satellite i to receiver A (in electrons/m²).

The ionosphere TEC can be reconstructed from the so-called geometric free combination $\varphi_{A,GF}^i$:

$$\varphi_{A,GF}^i = \varphi_{A,L1}^i - \frac{f_{L1}}{f_{L2}} \varphi_{A,L2}^i \tag{2.3}$$

Based on equation (2.1) and equation (2.2), equation (2.3) can be rewritten in function of the slant TEC from receiver A to satellite i, TEC_A^i (Warnant et al, 2000):

$$\varphi_{A,GF}^i = 0{,}552\ 10^{-16}\, TEC_A^i + M_{A,GF}^i + N_{A,GF}^i + \varepsilon_{A,GF}^i \tag{2.4}$$

Where $N_{A,GF}^i$, $M_{A,GF}^i$ and $\varepsilon_{A,GF}^i$ are respectively the geometric free ambiguity, multipath and noise:

$$N_{A,GF}^i = N_{A,L1}^i - \frac{f_{L1}}{f_{L2}} N_{A,L2}^i$$

$$M^{i}_{A,GF} = M^{i}_{A,L1} - \frac{f_{L1}}{f_{L2}} M^{i}_{A,L2} \tag{2.5}$$

$$\varepsilon^{i}_{A,GF} = \varepsilon^{i}_{A,L1} - \frac{f_{L1}}{f_{L2}} \varepsilon^{i}_{A,L2}$$

This combination is called "geometric free" due to the fact that it does not contain geometric terms (i.e. satellite and receiver coordinates). Therefore, it cannot be used to compute the user position. In the absence of cycle slips, the real (non-integer) ambiguity $N^{i}_{A,GF}$ has to be solved for every satellite pass.

From Equation (2.4), it can be seen that, if we neglect multipath and noise, the geometry-free combination also allows monitoring the time variation of the TEC, e.g. $\Delta TEC^{i}_{A}(t_k)$:

$$\Delta TEC^{i}_{A}(t_k) = 1.812 \; \frac{\left(\varphi^{i}_{A,GF}(t_k) - \varphi^{i}_{A,GF}(t_{k-1})\right)}{\left(t_k - t_{k-1}\right)} \tag{2.6}$$

where

t_{k-1} and t_k are 2 consecutive measurement epochs;

$\Delta TEC^{i}_{A}(t_k)$, measured in TECU/min, is defined as:

$$\Delta TEC^{i}_{A}(t_k) = \frac{TEC^{i}_{A}(t_k) - TEC^{i}_{A}(t_{k-1})}{\left(t_k - t_{k-1}\right)} \tag{2.7}$$

It is important to stress that the computation of $\Delta TEC^{i}_{A}(t_k)$ does not require the estimation of the real ambiguity, $N^{i}_{A,GF}$, as long as no cycle slip occurs. Equation (2.6) can be used to detect high frequency changes in the TEC due to irregular smaller-scale ionospheric phenomena.

The slant gradients computed by equation (2.6) are then verticalized by using a mapping function *M* and a simplified representation of the ionosphere. This representation consists on liken the ionosphere to a thin spherical layer (the *ionospheric shell*) which contains all the electrons coming from the ionosphere. The ionospheric shell is placed at an ionospheric height *h*, which is the height between the thin shell and the ground surface; in our work, *h* is fixed at 400 km. The intersection between the line-of-sight "satellite-station" and the ionospheric shell is called the *Ionospheric Pierce Point* (IPP); so, to each measure of the gradients corresponds an IPP. Vertical gradients are computed as follows:

$$\Delta TEC_A^i(t_k)_{Verticalized} = \Delta TEC_A^i(t_k) \cdot M \tag{2.8}$$

with

$$M = \cos(z_{IPP})$$
$$M = \cos\left(\arcsin\left(\frac{R_T \sin(z)}{(R_T + h)}\right)\right) \tag{2.9}$$

if R_T is the Earth radius (R_T = 6371 km) and z is the zenithal angle of the satellite at the station. Angle z_{IPP} is the zenithal angle of the satellite at the IPP.

The time derivation at different elevations when tracking a satellite introduces an artificial trend, not connected with the ionospheric variability, but due to the geometry of the satellite orbit. In order to remove the trend, we filter out the low frequency changes in the TEC by modeling verticalized ΔTEC_A^i using a low order polynomial. The residuals of this adjustment (i. e. verticalized ΔTEC_A^i - polynomial) contain the higher frequency terms and are called Rate of TEC (*RoTEC*).
Then, the standard deviation of the residuals, σ_R, is computed, separately for every satellite in view, on 15 minute periods. When σ_R > 0.08 TECU/min (on a 15 minute period), we decide that an "*ionospheric event"* is detected. In addition, an "*ionospheric intensity"* is associated to every ionospheric event: the intensity of the event (the amplitude of the associated TEC variations) is assessed based on a scale which ranges from 1 to 9 depending on the magnitude of σ_R. This quantity is a measure of amplitudes of the small-scale irregularity structures, effectively degrading the accuracy of the GNSS differential positioning techniques.
The choice of the threshold value of 0.08 TECU/min comes from the fact that the multipath can also give rise to high frequency changes in the geometric-free combination. This site-dependent effect can reach several centimetres on phase measurements and has periods ranging from a few minutes to several hours depending on the distance separating the reflecting surface from the observing antenna (if this distance is shorter, the period is longer). The multipath effect being more frequent at low elevation, we have chosen an elevation mask of 20°. In the case of the Brussels permanent GPS station (on which the present study is based), a threshold value of 0.08 TECU/min is large enough to avoid interpreting multipath effects as ionospheric phenomena. This value should be valid for most of the GPS sites but should be applied with care in locations where the multipath is particularly important.
All the details concerning this technique (including the choice of the thresholds) are discussed in Warnant (1998) and Warnant et al. (2000).

2.2. Types of structures observed in Europe at mid-latitudes

This methodology outlined in paragraph 2.1 has been applied to the continuous measurements collected at Brussels since April 1993.

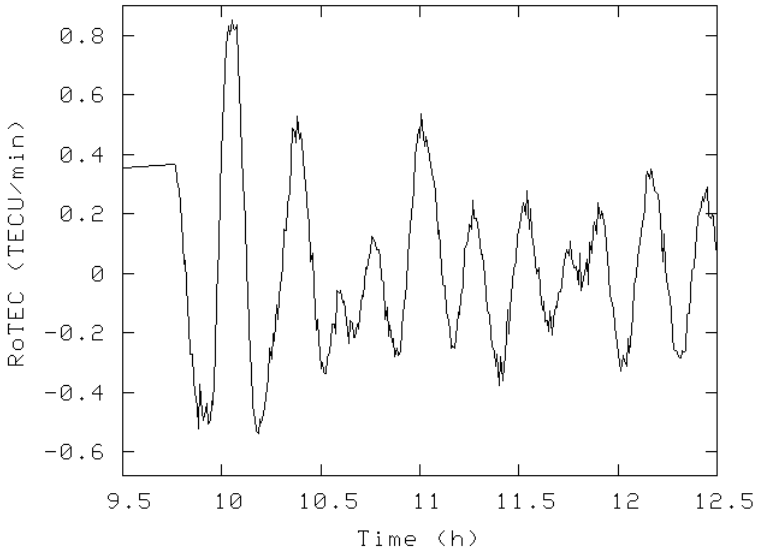

Figure 2.1. Vertical TEC variability (rate of change in TECU/min) due to a TID observed at Brussels along the track of satellite 7 on DOY 340 in 2001.

From this study, it appears that TEC smaller-scale variability at mid-latitude (in Europe) is mainly related to two types of phenomena: Travelling Ionospheric Disturbances (TID's) or "noise-like" variability. TID's appear as waves in the electron density which is due to interactions between the ionosphere and the neutral atmosphere. They have wavelengths ranging from a few km to more than thousand km and periods of a few minutes up to 3 hours. Figure 2.1 shows the variability in vertical TEC (vertical TEC rate of change) due to a TID detected at Brussels on DOY 340 in 2001 (December 6 2001).

In mid-latitude stations, "noise-like" variability in TEC can also be observed. Such variability is mainly detected during geomagnetic storms. Figure 2.2 shows "noise-like" variability in vertical TEC due to a geomagnetic storm observed at Brussels on DOY 324 in 2002 (November 20 2002). The signature of these "noise-like" structures in TEC is very similar to the signature of scintillations which are variations in phase and amplitude of GNSS signals due to the presence of irregularities in the ionosphere electron concentration. Scintillations are only observed in the equatorial and in the polar regions but noise-like variability observed at mid-latitude during severe geomagnetic storms can also induce strong degradations in GNSS differential applications.
Warnant et al. (2007-1), Warnant et al. (2007-2) and Hernandez-Pajares et al. (2006) analyse in more details the ionospheric and geomagnetic conditions under which such variability appears mainly based on ionograms, GPS-TEC and geomagnetic measurements.

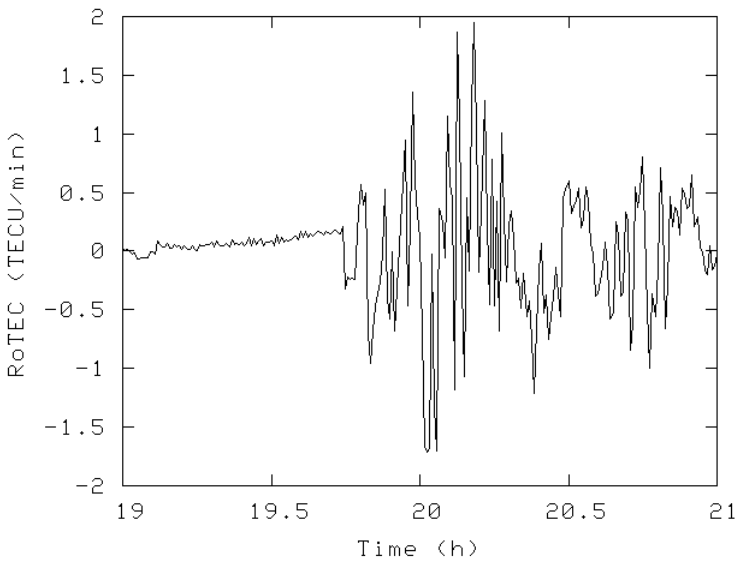

Figure 2.2. Noise-like variability in vertical TEC rate of change (in TECU/min) observed at Brussels during a geomagnetic storm on November 20 2002 along the track of satellite 22.

3. INFLUENCE OF CYCLE SLIPS

3.1. Introduction

In order to attain high precision in applications using GPS phase measurements, it is necessary to detect and remove cycle slips.

A cycle slip can be defined as a sudden jump (always an integer number of cycles) in the carrier phase observable. In fact, there are three main sources for cycle slips. Firstly (and most frequently), a cycle slip can be due to an obstruction of the satellite signal by some obstacles (trees, buildings…). Secondly, this can be due to a low signal-to-noise ratio caused by bad ionospheric conditions, multipath… Thirdly, a failure in the receiver software can cause a cycle slip.

All cycle slip detection processes are based on quantities derived from the observations, namely on linear combinations of the undifferenced carrier-phase (φ_1 and φ_2) and pseudorange (P_1 and P_2) observations. Once the times series of the derived quantities have been computed, the cycle slip detection process consists in detecting discontinuities in those times series.

Here, we use a cycle slip detection process in the preprocessing step of the "GPS-TEC" software (computation of the TEC and the TEC variability). It is then particularly important to adequately detect the cycle slips, in order to be sure that the ionospheric data are all there (no cycle detected instead of ionospheric variability) and correct (no cycle slip remaining).

3.2. Original method

3.2.1. Principles

In the original "GPS-TEC" software, we use a cycle slip detection process based on Kalman filtering based on two different linear combinations: the phase-range combination and the geometric-free phase combination.
In fact, we can form two mono-frequency phase-range combinations (RP_1 and RP_2) which can be written as follows:

$$RP_1 = \varphi_1 - \frac{P_1}{l_1}$$

$$RP_2 = \varphi_2 - \frac{P_2}{l_2}$$

with l_i the corresponding wavelength.
Because depending on pseudorange measurements, this combination has a relatively high noise level. Moreover, it depends on the ionospheric effects, which can lead to important epoch to epoch variations in the combination.
The dual-frequency geometric-free phase combination φ_{GF} can be written as follows:

$$\varphi_{GF} = \varphi_1 - \frac{f_1}{f_2}\varphi_2$$

with f_i the corresponding frequency.
This combination is independent of the pseudorange measurements and is consequently a smoother quantity than the phase-range combination. However, it also depends on the ionospheric effects which can cause epoch to epoch changes.

3.2.2. Problems

As our objective is to characterize ionospheric activity, this original cycle slip detection process is not well adapted because it only uses ionospheric dependent data combinations. In case of high ionospheric activity, it is therefore really difficult to decide whether the changes in the data combination are due to cycle slips or to the ionospheric activity. As a consequence, there is a risk of interpreting abrupt changes in the considered combination as cycle slips when these changes are due in reality to ionospheric variability. In this context, even if the existing software was giving satisfying results in usual conditions, we noticed that during extreme ionospheric activity periods, this software was interpreting ionospheric variability as successive cycle slips and was removing long periods of data. This is a major problem due to the fact that the goal of our work is to detect and study period with strong ionospheric activity.
Figure 3.1 and 3.2 illustrate the problem encountered with the existing cycle slip detection method; Figure 3.2 shows the data remaining after cycle slip detection with the old method: when the ionospheric variability increases above 1.5 TECU/min, the software interprets the data as successive cycle slips and removes these data. Figure 3.2 shows the same data but the threshold for cycle slip detection on the geometric free combination has been arbitrarily increased up to 10 cycles: the ionospheric variability is

not interpreted as cycle slip but in this way, there is an important risk to have remaining cycle slips in the data which could be interpreted as ionospheric variability. Therefore, we have developed and implemented a new method for cycle slip detection.

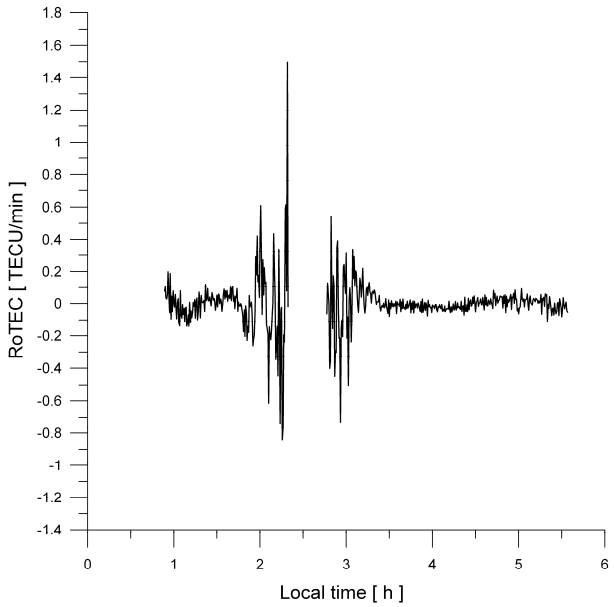

Figure 3.1. Ionospheric variability at BRUS – DOY 033/2002 – Satellite 8 Usual threshold for cycle slip detection

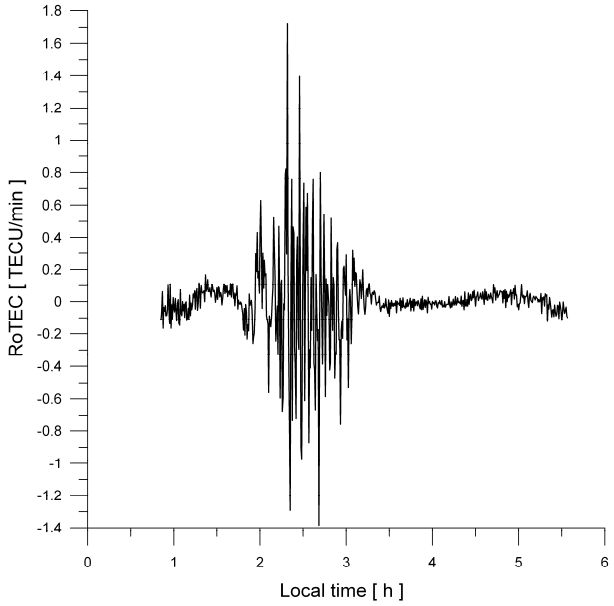

Figure 3.2 Ionospheric variability at BRUS – DOY 033/2002 – Satellite 8 Increased threshold for cycle slip detection

3.3. New method

3.3.1. Principles

Therefore, in a second step, we have developed an improved cycle slip detection process based on the widelane phase minus narrowlane pseudorange combination ($\varphi_{WL\text{-}NL}$).

$$\varphi_{WLNL} = \varphi_1 - \varphi_2 - \frac{f_1 - f_2}{f_1 + f_2}\left(\frac{f_1}{c}P_1 + \frac{f_2}{c}P_2\right) = N_2 - N_1 - \frac{f_1 - f_2}{f_1 + f_2}\left(d_{12} + M_{12} + s_{12}\right)$$

As we can see, this combination consists of the widelane ambiguity $N_{12} = N_2 - N_1$, a residual code hardware delays term d_{12}, a residual code multipath term M_{12} and a residual code noise term s_{12}.
For cycle slip detection purpose, the main advantage of this combination is its independence of the ionospheric effects.
However, the noise of this observable makes cycle slip detection unlikely[1]. That's why we have to apply a running average filter (or low-pass filter) to this combination so that the residuals terms average down to more or less constant values.
Let us present the main steps of the WL-NL cycle slip detection process applied:

1. First, we compute the recursive mean μ and the recursive standard deviation σ. The term recursive means that the mean and the standard deviation are computed and updated epoch by epoch.

2. Then, we calculate the relative confidence interval $\boxed{\mu \pm 4\sigma}$.

3. If the current value of the WL-NL combination is outside that interval, the data is declared to be an "outlier".

4. If there are two consecutives outliers, we declare that a cycle slip has occurred and all the parameters are reinitialized: we start a new period and define a new ambiguity term.

5. If there is just one isolated outlier, it is removed from the data set but the parameters are not reinitialized.

Another advantage of this method is that it only uses statistical information from the data themselves, without the need of initializing parameters like in the Kalman filtering technique.

Figure 3.3 and 3.4 show the WL-NL combination in function of time in two different cases.

[1] The measurement noise of this combination is still lower than that of the phase-range combination *RPi*.

In figure 3.3 we can see that the WL-NL combination remains inside the confidence interval, except for two isolated points: two "outliers". Those outliers are then removed from the data set. In figure 3.4, we can clearly identify a cycle slip, which is confirmed by the fact that the combination is outside the confidence interval during two consecutive epochs.

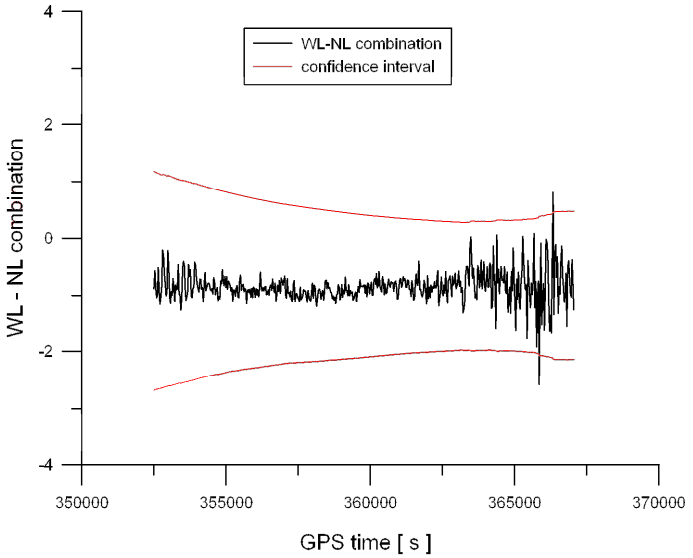

Figure 3.3 WL-NL combination at DENT – DOY 324-03 – Satellite 13

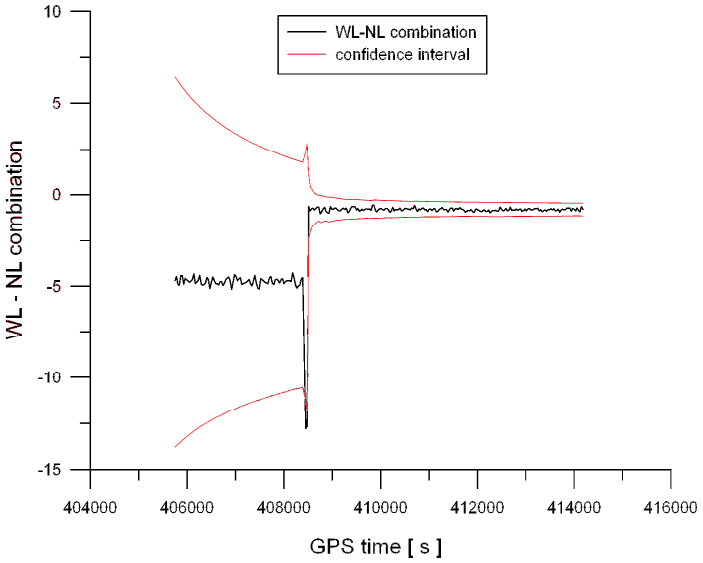

Figure 3.4 WL-NL combination at BATT – DOY 324-03 – Satellite 2

3.3.2. Analysis

In theory, one combination is sufficient for detecting cycle slips. But the characteristics of the WL-NL combination do not allow detecting a cycle slip whose value would be equal on φ_1 and φ_2. For those events – which are known to be relatively rare –, we should use a second combination in the detection process. But this combination (for example φ_{GF}) would automatically be dependent on the ionospheric effects, causing all the problems mentioned above.
In this context, instead of implementing a new combination, we will verify that the ionospheric variability values computed using the mew method do not result from bad cycle slip detection and that it can be considered as real ionospheric variability. That point is particularly crucial in case of geomagnetic storm.
We have concentrated our analysis on the geomagnetic storm of DOY 324/03 (20/11/2003) for different stations, and precisely on t = 408480 s (GPS time) and t = 408510 s (for the satellites concerned). Contrary to the original method (figure 3.5), the new method do not detect cycle slips at BRUS at those epochs (and then do not delete data), which finally leads to very important ionospheric variability values (figure 3.6).

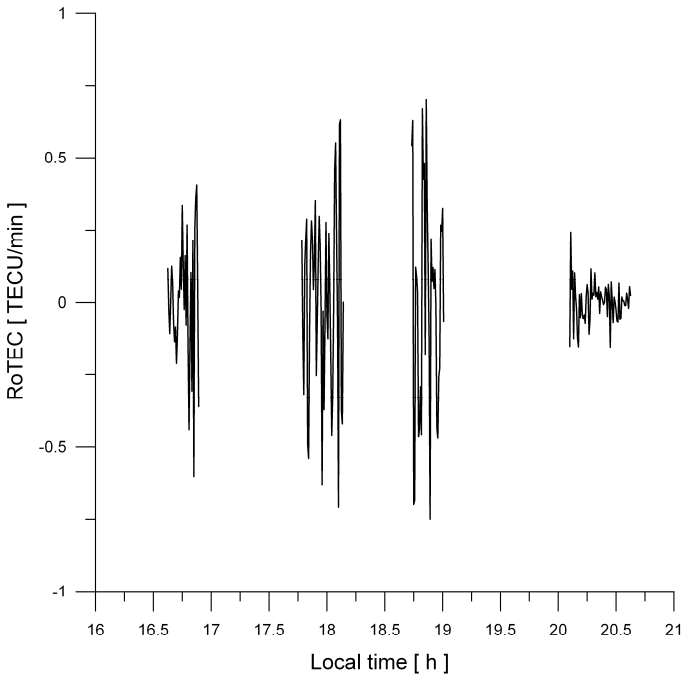

Figure 3.5. Ionospheric variability at BRUS – DOY 324/2003 – Satellite 2
Original cycle slip detection method used

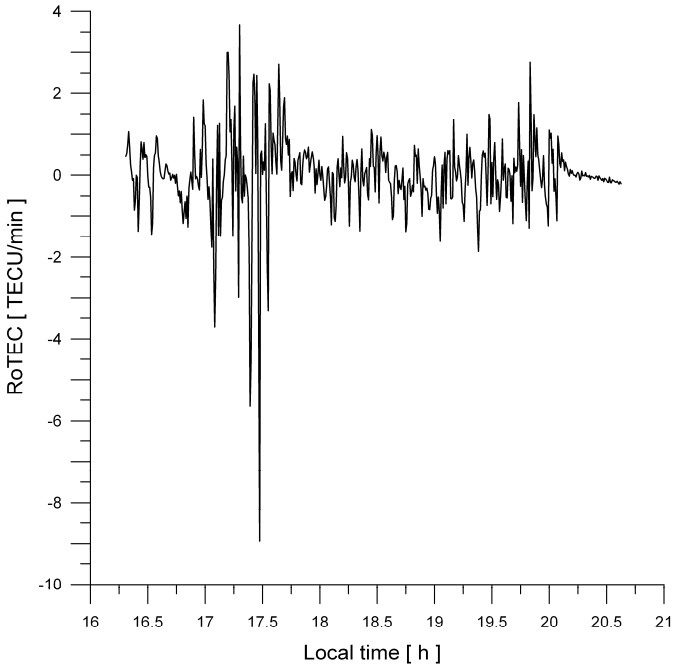

Figure 3.6. Ionospheric variability at BRUS – DOY 324/2003 – Satellite 2
New cycle slip detection method used

We will try to prove that the ionospheric variability in figure 3.6 is real and not created by a cycle slip missed by the detection technique (i.e. equal on φ_1 and φ_2). On this basis, we have analyzed several cases and parameters in order to be able to give several arguments ("ionospheric arguments") and counter-arguments ("pro cycle slip" arguments).

First here are the "pro cycle slip" arguments:

1. We can show that the influence of a cycle slip on φ_{GF} equals (– 0.28) * the value of the cycle slip, which is approximately the case here.
2. We can see that the phenomena appear at the same time in different stations (BRUS,DOUR,DENT,GILL…), which could be due to cycle slips caused by the ionospheric variability at the same time in the different stations.

Now let us develop the "ionospheric" arguments (with the corresponding numbering):

1. We can show that the influence of the ionospheric effects on φ_{GF} equals (– 0.32) * the value of the effect on RP_1, which is the case here.
2. We can see that the phenomena appear at the same time in different stations (BRUS,DOUR,DENT,GILL…), which could be due to ionospheric variability (approximately the same conditions at the same time).
3. The RP_1 and RP_2 variations (at those epochs) are not exaggerated with regards to the possible ionospheric variability. Those changes are probably due to

ionospheric variability and not to cycle slips (which can cause random – and thus larger – slips).

4. The new method detects cycle slips at those critical epochs in BDN stations (like GILL,BATT…) which are equipped with LEICA GPS receivers and not in stations like BRUS,DENT… which are equipped with Ashtech GPS receivers. That point can be explained by the difference between the receivers at those stations. The receivers of the first group of stations (LEICA receivers) are more sensible to the ionospheric noise than those of the second group (ASHTECH receivers).
5. We can observe the same ionospheric variability structures for the different satellites and for the different stations.
6. When analyzing the IF (ionospheric free) and GF (geometric free) double-differenced phase measurements, there is no cycle slip detected for BRUS/DOUR or BRUS/DENT. Due to the ionospheric variability, the DD-GF combination is well noisy but there is no "jump" visible. For BRUS/GILL, we can however detect a cycle slip on both combinations (DD-IF and DD-GF), which confirms the fact that a real cycle slip occurs at GILL (it is detected by our new method) and not in BRUS for example.

All those "ionospheric" arguments show that the ionospheric variability of DOY 324/03 is real and not created by missed cycle slips. That confirms the validity of our developed technique.

3.4. Conclusions

After analyzing the original cycle slip detection technique, we have concluded that it is not possible to improve it. In fact, we would not be able to determine the origin of the changes in the times series of the derived quantities (because of their dependence on the ionospheric effects): a cycle slip or the ionospheric variability? However, it is crucial because our objective is to use the data for TEC computing and analyzing.
For this reason, we have developed a new cycle slip detection technique based on running average filtering of the widelane-narrowlane combination. This combination has the advantage not to be dependent on the ionospheric effects and, even if it cannot detect equal cycle slip on φ_1 and φ_2 that method gives reliable results.

4. SMALL-SCALE DISTURBANCE "CLIMATOLOGY"

4.1. Number of events – Probability of occurrence

Figure 4.1 shows the number of "ionospheric events" (as defined above) detected per month at Brussels from January 1994 to December 2006. Most of these "events" are due

to Travelling Ionospheric Disturbances (as already said, “noise-like” phenomena are mainly observed during geomagnetic storms).

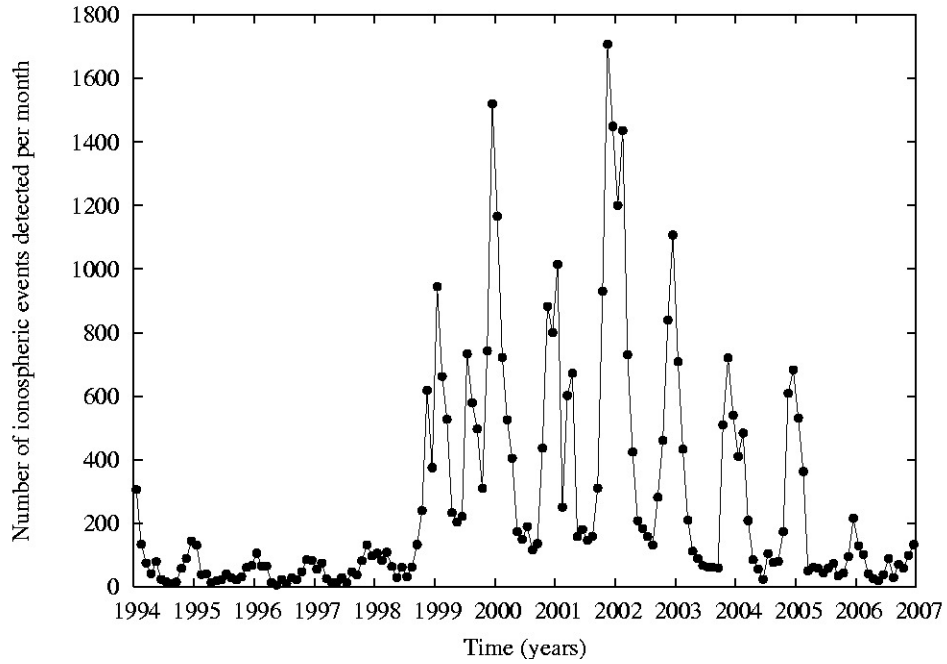

Figure 4.1 Number of detected ionospheric events per month at Brussels from January 1994 to December 2006.

The analysis of figure 4.1 shows that:

- TID’s are frequently observed all the time (during all seasons and during all phases of the 11-year solar activity cycle).
- The number of detected events has an annual peak during winter time independently of solar activity but the peak is much sharper at solar maximum.
- The number of TID’s strongly depends on the solar activity cycle: for example, about 100 events were observed in December 1996, at solar minimum when more than 1500 events were detected in December 1999 and in November 2001 at solar maximum (the 2 peaks which are present in figure 4.1 correspond to the peaks of 2000 and 2002 observed in solar cycle 23).

We can increase the temporal resolution from one month to one day in order to display the number of detected events per day. Figure 4.2 shows the evolution of the daily number of detected events from January 1994 to December 2006 (solar cycle 23). We can easily identify the most disturbed days (“worst cases”) in terms of ionospheric effects; moreover, table 1 contains the ten most disturbed days from 1994 to 2006 in terms of ionospheric events. The analysis of figure 4.2 and table 1 shows that the days that present a large number of events are mainly days where geomagnetic storms occurred. However, TID’s can induce strong ionospheric events and be at the origin of highly disturbed days.

For example, DOY 034/02 is the fifth most disturbed day between 1994 and 2006 with 153 ionospheric events and an associated maximum TEC variability of 0.96 TECU/min.

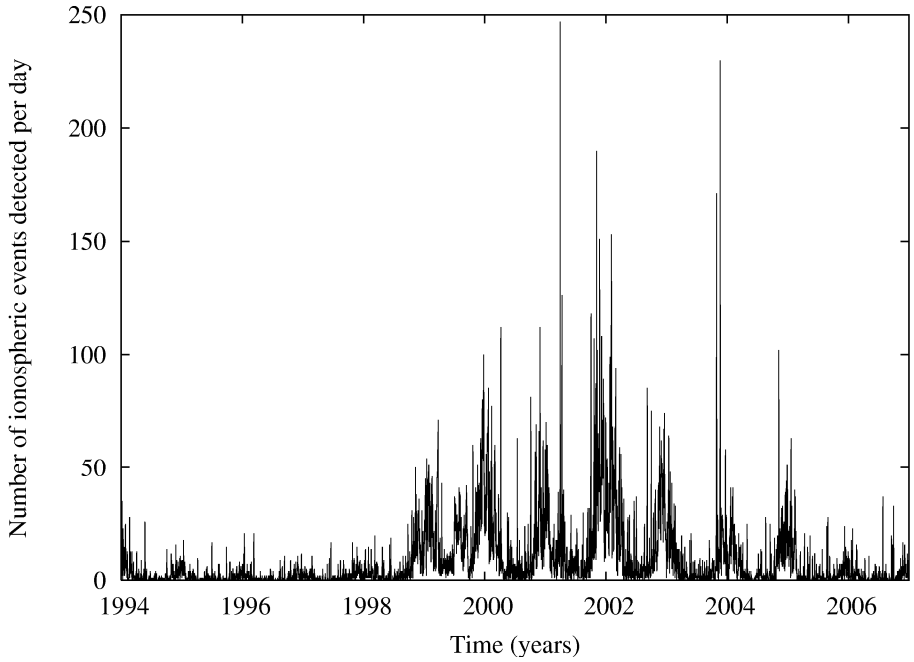

Figure 4.2 Number of ionospheric events detected per day at Brussels from January 1994 to December 2006.

	DOY	Date	Number of events	Cause	Kp max	DST min [nT]
1	090/01	2001/03/31	247	Geomagn. Storm (GS)	8.7	-358
2	324/03	2003/11/20	230	GS	8.7	-422
3	310/01	2001/11/06	190	GS	8.7	-277
4	303/03	2003/10/30	171	GS	9	-383
5	034/02	2002/02/03	153	TID	2	-30
6	328/01	2001/11/24	151	GS	8.3	-216
7	033/02	2002/02/02	139	multiple geomagnetic causes	4.7	-83
8	101/01	2001/04/11	126	GS	8.3	-256
9	302/03	2003/10/29	125	GS	9	-350
10	276/01	2001/10/03	118	GS	7	-182

Table 1. The 10 most disturbed days in terms of ionospheric events from 1994 to 2006

Ionospheric irregularities have also a dependence on season and local time. As it is shown in figure 4.3, ionospheric irregularities take mainly place during autumn and winter months. This result is verified for each phase of the solar cycle (minimum, maximum of activity).

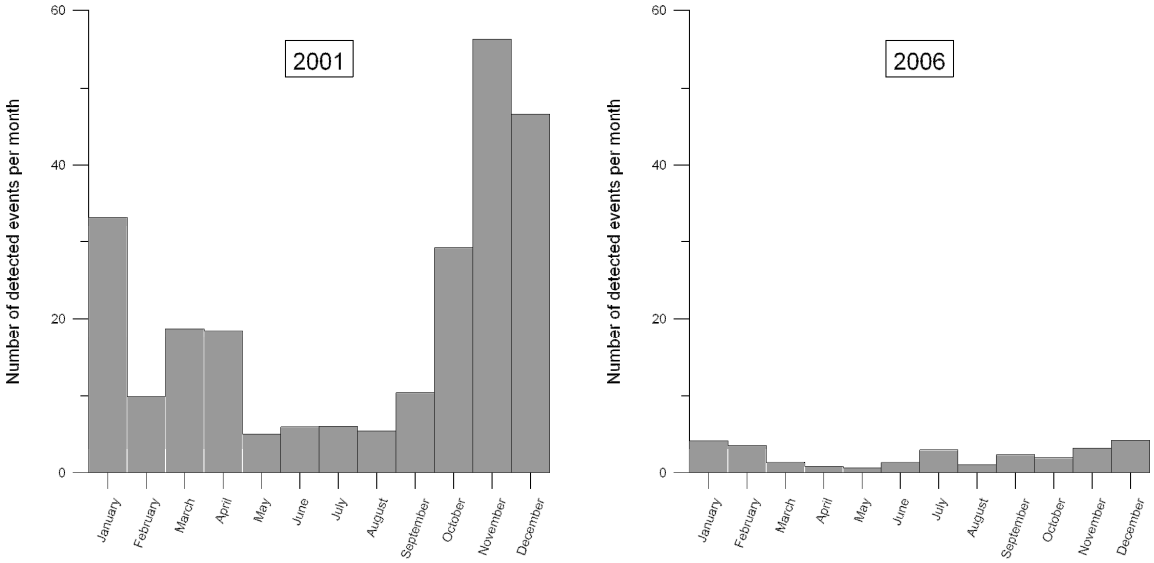

Figure 4.3 Number of ionospheric events detected per month at Brussels for the year 2001 (solar maximum) and the year 2006 (solar minimum).

However, the occurrence of irregularities depends also on local time: in figure 4.4 we divide local time in periods of 15 minutes (in other words, there are 96 periods for 24 hours) and we show the total number of events which occurred in 2001 (left) and in 2006 (right) for each 15 minutes period. First, we'll analyze the year 2001 in order to characterize the mean behavior of the ionosphere during solar maximum. Then, the incidence of a low solar activity (2006) is analyzed.

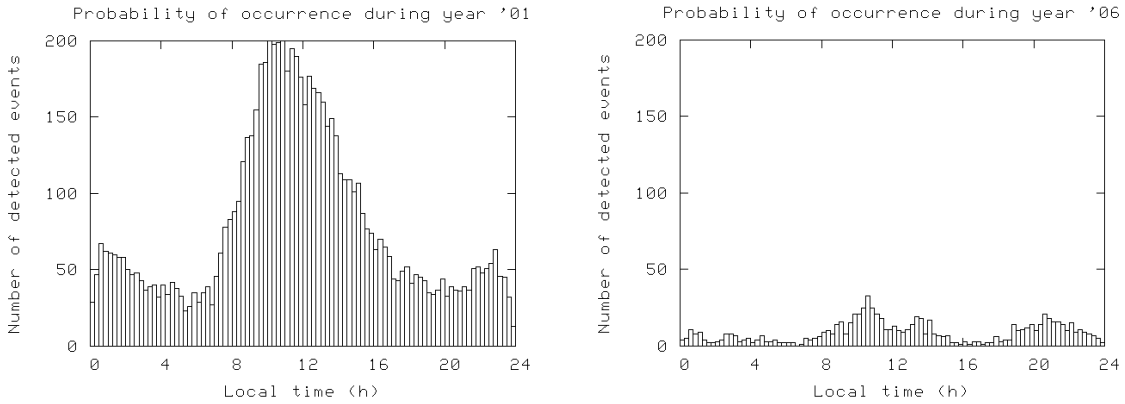

Figure 4.4 Ionospheric events distribution at Brussels for the year 2001 (solar maximum) and the year 2006 (solar minimum) in function of local time.

4.1.1. High solar activity (2001)

The analysis of the figure 4.4 (left) shows that most of irregularities occur around 10 A.M. There is also a secondary maximum observed during the night around 1 A.M. The periods characterized by a minimal ionospheric activity are located in the early morning (around 6 A.M.) and in the late afternoon (about 6 P.M.). This annual behavior can be divided into the four seasonal behaviors as we can see in figure 4.5. We can say that up to 50% of the annual number of ionospheric irregularities is produced during autumn; furthermore, let us note that winter behavior is quite similar to the autumn's one.
In spring and summer, there are nearly no irregularities detected (in comparison with autumn and winter) and the behavior seems to be independent of local time.

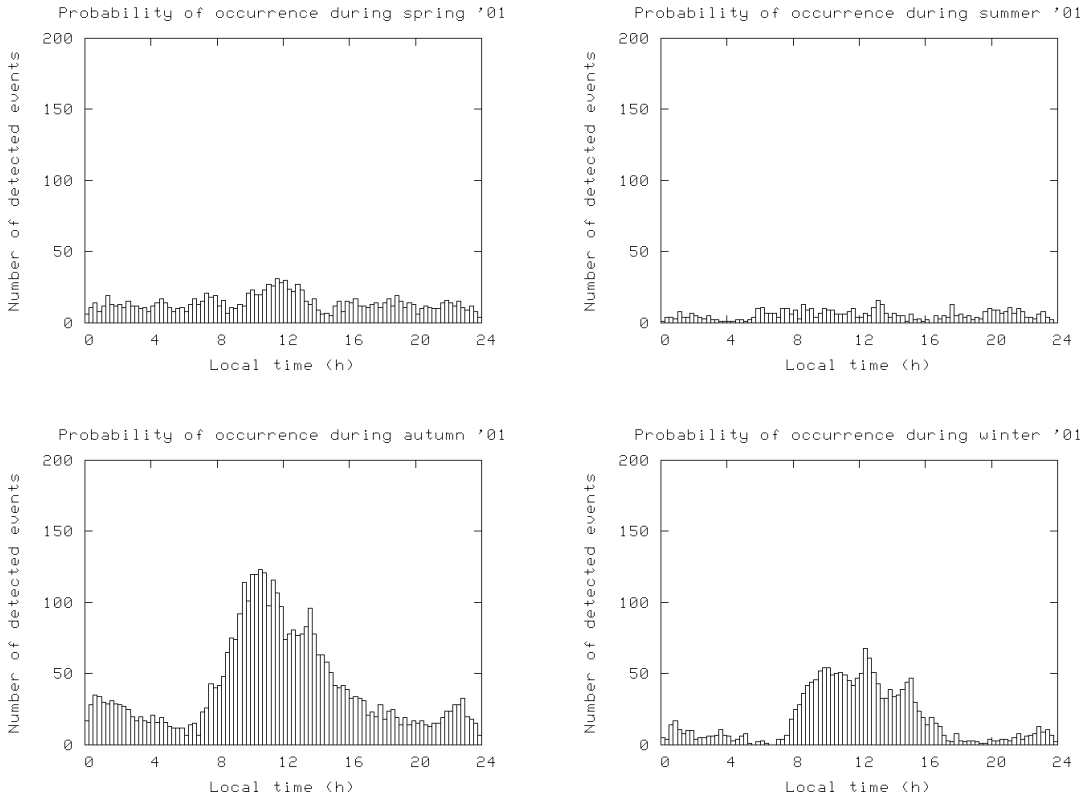

Figure 4.5. Ionospheric events distribution in 2001 in function of the season and local time

4.1.2. Low solar activity (2006)

Figure 4.4 (right) shows three peaks: two around noon (main peak at 10 A.M. and secondary peak at 1 P.M.) and the third around 8 P.M. The minimal activity is still localized early in the morning and in the afternoon. Let us also note that the number of detected events is very low in comparison with the number of events detected during the

year 2001 at Solar maximum. As for the year 2001, let us decompose the annual distribution into the four seasonal behaviors; this is shown at the figure 4.6.

As for the year 2001, we can clearly observe that months of autumn and winter explain the major part of the annual distribution of the events in function of time. Nevertheless, the major part of the third peak comes from the summer days: there are nearly no irregularities during daytime in summer but the occurrence of such phenomena take place at sunset. This phenomenon was not visible for the year 2001.

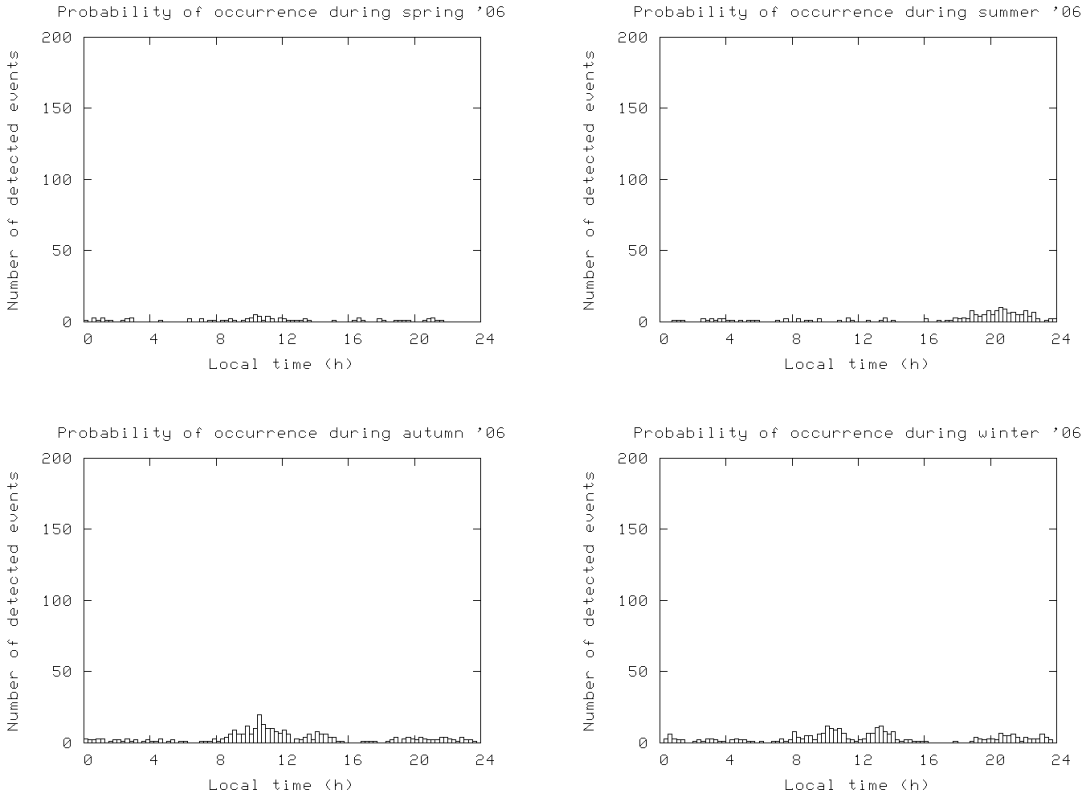

Figure 4.6 Ionospheric events distribution in 2006 in function of the season and local time.

4.1.3. <u>TID's and noise-like structures</u>

Ionospheric events presented in the previous statistics are mainly caused by TID's and noise-like structures (NLS); we can try to separate these two components if we assume that NLS are due to disturbed geomagnetic conditions. We made the same statistics as previously (i.e. analysis of the ionospheric events distribution in function of local time) but only by using the days with no geomagnetic activity. In reality, we removed from our statistics the days that present a maximum daily value of index Kp equal or greater than 5; so we excluded all stormy days.
Figure 4.7 shows a similar graph than in figure 4.4 but when considering only days with $Kp_{daily\ max} < 5$.

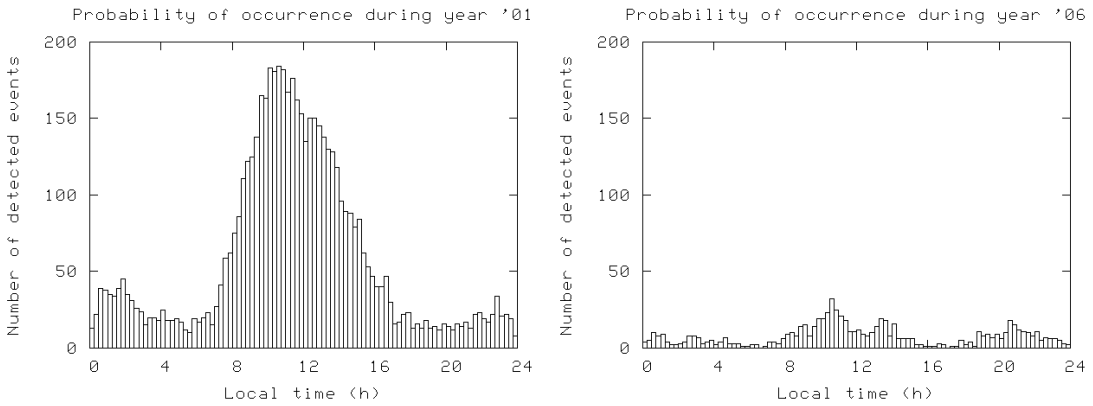

Figure 4.7 Ionospheric events distribution at Brussels for the year 2001 (solar maximum) and the year 2006 (solar minimum) in function of local time. All days included present $Kp_{daily\ max}$ <5.

The comparison between figures 4.7 and 4.4 shows that the shape of the distribution is similar if we include or not the days where geomagnetic storms occurred. In fact, stormy days induce an offset of the number of events detected; this means that noise-like structures due to geomagnetic storms occur all the time, contrary to the TID distribution that shows a specific shape with a maximum around 10 A.M.

4.1.4. Conclusions

The number of ionospheric irregularities depends mainly of the solar activity: irregularities are most frequently observed during high solar activity periods, like in 2001 or in 2002.
Moreover, the distribution of these structures differs from seasons and depends on local time; we have identified two main types of irregularities:

- those which occur during daytime (around noon), mainly during autumn and winter months;
- those which occur at sunset (around 8 P.M.), mainly during summer. Let us remind that these kinds of structures have only been detected during the year 2006 (i.e. during a year of solar minimum) because 2006 is the only year where a peak in the distribution is clearly visible. These irregularities are also less numerous than irregularities which occur during daytime.

We showed that the major part of the irregularities detected at Brussels seems to be TID's; these structures are responsible for the shape of the temporal distribution, contrary to the noise-like structures which occur all the time.

4.2. Amplitude of TEC time derivative

The largest rate of TEC (TEC time derivative) detected at Brussels during the period 1994-2006 were observed during geomagnetic storms on October 30 2003 (303/03) and November 20 2003 (324/03). In both cases, *vertical TEC variability of more than 8 TECU/min was measured.*

4.2.1. Maximum Rate of TEC (RoTEC)

Between January 2001 and December 2006, we analysed the maximum daily Rate of TEC (RoTEC) value. We have afterwards grouped these values according to the seasons: we obtained the maximum seasonal RoTEC values which appear in the table 2. Let us note that all these daily values have been validated by verifying that they do not correspond to bad data values (outliers).

	Spring	Summer	Autumn	Winter
2001	6.881	1.122	4.028	9.068
2002	0.745	1.821	1.946	2.211
2003	0.693	0.653	9.839	1.231
2004	1.581	1.152	0.861	1.263
2005	1.234	2.579	0.503	1.276
2006	0.582	1.197	0.805	0.845

Table 2. Maximum seasonal RoTEC values at Brussels from January 2001 to December 2006 (expressed in TECU/min).

The largest gradients in TEC detected at Brussels were observed during severe geomagnetic storms. For example, the storm of the DOY 303/03 (30th October 2003) which presented a DST minimum index of –383 nT was responsible for the largest TEC gradients observed during the period 1994-2006: 9.839 TECU/min.
TID amplitude is by far smaller than the amplitude due to geomagnetic storms: the analysis of a lot of TID cases shows that the maximum RoTEC value observed during the occurrence of a TID was about 1.5 TECU/min. Nevertheless, let us remind that we did not analyse all days where a TID occurred.
Moreover, the analysis of table 2 shows that strong irregularities occur even during solar minimum, for example in summer 2006 where gradients up to 1.2 TECU/min were reached. Besides, let us underline that this maximum value of summer 2006 was larger than the maximum value of summer 2001 (solar maximum). This means that, even during periods where the probability of occurrence of ionospheric irregularities is very low, large TEC gradients can occur.

A third cause of ionospheric variability is the electromagnetic radiation (flash) due to solar flares and especially from the extreme-UV (EUV) and soft X-rays. The ionization caused by these flashes reaches very high values so that TEC is strongly affected. These effects are assessed in the next section.

4.2.2. Worst case study : 301/03 and 303/03

The two intense events of 28 and 30 October 2003 are due to different causes:

- the event of 301/03 is caused by the most powerful solar flare ever observed in EUV;
- the event of 303/03 is due to a severe geomagnetic storm which is the origin of the largest RoTEC values ever measured at Brussels since 1994.

DOY 301/03 (28/10/03)

The solar flare which occurred at 11h00 UTC was the most powerful in EUV (since the beginning of the measurements of SOHO/CELIAS-SEM) and the fourth intense in X-rays (type X17.2 according to NOAA). Figure 4.11 shows an example of the effects of this solar flare on TEC and on the RoTEC (satellite 7); all visible satellites present exactly the same behavior.
When considering the value of TEC before the flare, we can assess that it caused an increase in TEC of about 30%. TEC gradients for satellite 7 reached 4.7 TECU/min but the satellite 29 presents a maximal variability of 5.1 TECU/min.

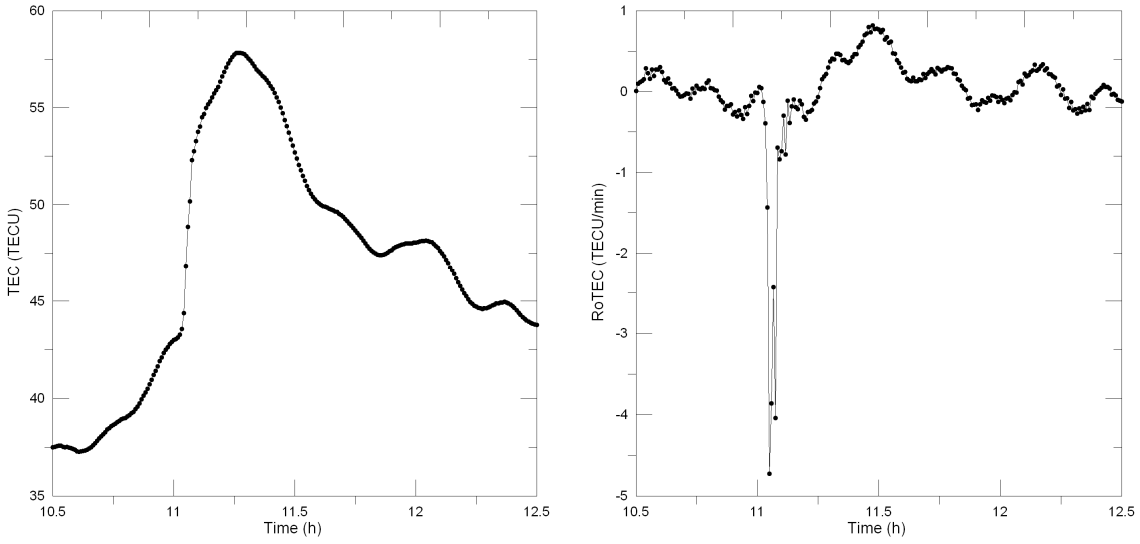

***Figure 4.11 Effects of the solar flare of 28/10/03 on the TEC (left) and on the RoTEC (right) at Brussels (satellite* 7).**

DOY 303/03 (30/10/03)

This geomagnetic storm which occurred on 30/10/03 was due to a Coronal Mass Ejection (CME) produced 24 hours before; it was characterized by a Dst value of -383 nT and Kp values of 9 during 6 hours. This storm caused the largest temporal gradients in TEC ever observed at Brussels since 1994: the extreme value reached about 9.8 TECU/min (figure 4.12).

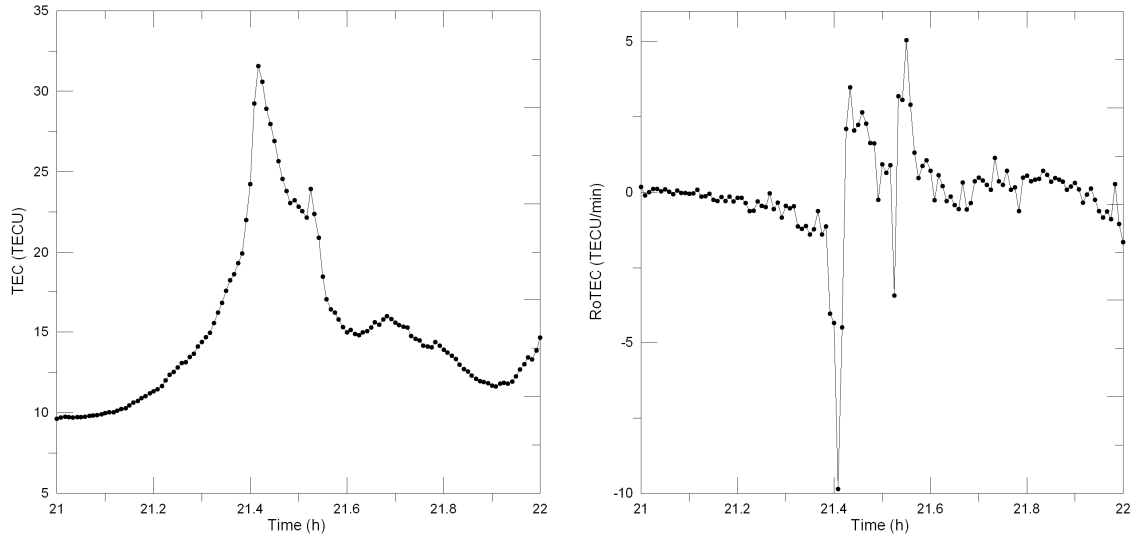

Figure 4.12 Effects of the geomagnetic storm of 30/10/03 on the TEC (left) and on the RoTEC (right) at Brussels (satellite 31).

4.3. Sensitivity test

4.3.1. Extreme RoTEC values

The maximum RoTEC values shown in the previous sections depend on different parameters as the height of the ionospheric shell (h) or the elevation cut-off angle (E). Default values used to obtain our RoTEC values are h=400 km and E=20°.
The influence of these parameters on the computing of RoTEC must be assessed in order to test the sensitivity of our program.

1) The influence of the height of the ionospheric shell can be explained as follows: to bring the slant TEC gradients to vertical values, we need to know the zenithal angle of the satellite at the ionospheric pierce point (IPP). Precisely, this angle depends on the height of the ionospheric shell (see equation 2.9).
2) The elevation cut-off angle plays a role during the computing of the polynomial which fits the temporal series of the vertical TEC gradients ($\Delta TEC_{verticalized}$): the weaker the cut-off angle is, the more data points are available to compute the

polynomial. Therefore, RoTEC values which correspond to ($\Delta TEC_{verticalized}$ − polynomial) have different values if we change the cut-off angle.

We studied the maximum daily RoTEC value for the day 324/03 with different values of *E* and *h*. The results are shown in table 3.

		Ionospheric height [km]					
		200	**300**	**400**	**500**	**600**	**700**
Cut-off angle [°]	**10**	8.677	8.770	8.859	8.944	9.024	9.101
	15	8.709	8.807	8.900	8.988	9.072	9.152
	20	8.739	8.839	8.933	9.023	9.108	9.189
	25	8.775	8.877	8.973	9.063	9.149	9.231
	30	8.810	8.912	9.008	9.100	9.186	9.268

Table 3. Maximum daily RoTEC (in TECU/min) for DOY 324/03 in Brussels (BRUS) for different ionospheric heights and different cut-off angles.

We can observe that, for a fixed cut-off angle, the $RoTEC_{max,daily}$ is directly proportional to the ionospheric height. $RoTEC_{max,daily}$ is also directly proportional to the cut-off angle when considering a fixed ionospheric height. These results presented in table 3 show that the extreme value of 8.933 TECU/min obtained with the default values of the parameters (i.e. *h*=400 km and *E*=20°) is not quite different from the other values present in this table. Moreover, the maximum difference between two values in table 3 is about 0.6 TECU/min, i.e. about 7% of the mean $RoTEC_{max,daily}$.

In conclusions, we can affirm that our method is not very sensitive to these two parameters (*h* and *E*) in case of geomagnetic storm. As the extreme values of RoTEC are found during severe geomagnetic storm, we can say that our program is a fortiori reliable for smallest $RoTEC_{max,daily}$ values as it is the case for TID's where the amplitude is smaller than 1.5 TECU/min.

4.3.2. Number of ionospheric events

The number of ionospheric events as explained in section 2.1 is based on a time interval which within we compute the mean and the standard deviation of the residuals (RoTEC) in order to compute the ionospheric variability. The choice of the time interval is important because most of the ionospheric variability observed at mid-latitudes is due to TID's which have a characteristic period. By default, the period has been fixed at 15 min so that each period contains 30 data points because the sampling rate is 30s.

Firstly, we analyze the DOY 324/03 by changing the time interval and the cut-off elevation angle. Let us recall that one of the most powerful geomagnetic storm took place during this DOY 324/03. The results are presented in table 4.

		Time interval [min]					
		5	10	15	20	30	r²
Cut-off angle [°]	10	405	389	284	230	178	0.930092
	15	373	359	262	214	160	0.93787
	20	343	316	233	181	142	0.933127
	25	297	282	203	158	126	0.918569
	30	276	250	180	148	110	0.938884

Table 4. Number of ionospheric events detected for the DOY 324/03 (severe geomagnetic storm) for different time intervals and different cut-off angles

If we fix a cut-off angle, the analysis of table 4 shows that the number of ionospheric events is inversely proportional to the time interval. Inversely, if we fix the value of the time interval, we can see that the number of events decreases when the cut-off angle increases. This last observation is logical because lot of data are not taken into account when the cut-off angle is very high, which explains the fact that the number of observed ionospheric events is lower for a high value of this elevation angle.

As the relation between the number of ionospheric events and the time interval seems to be linear, let us try to model this dependency with a linear equation:

$$nb_{events} = a \cdot TI + b$$

with *TI* the time interval, *a* the slope of the linear regression and *b* the intercept. For each fixed value of the cut-off angle, these two constants *a* and *b* are different.

The percentage of the variability of nb_{events} explained by *TI* is the determination coefficient r^2 : we can see in table 4 that the linear regression explains about 93% of the total variance. This conclusion leads us to affirm that, in case of geomagnetic storm, there is clearly a linear relation between the time interval and the number of ionospheric events detected by our program. So, if we keep the same time interval for the whole analysis between 1994 and 2006, as it was the case in section 4.1 (*TI* = 15min), the results are not biased.

However, all the days analyzed between 1994 and 2006 do not present geomagnetic storm; that is the reason why we must study the evolution of the number of ionospheric events in function of time interval for a day where a TID occurred. Let us consider the DOY 359/04 where a TID of moderate amplitude ($RoTEC_{max} \approx 0.6$ TECU/min) happened. The methodology used in this study is the same as the one used for the DOY 324/03 (geomagnetic storm) and the results are shown in table 5.

We can say that there is no linear dependency between number of events and time interval as it was the case for the DOY 324/03. The time interval which offers the most ionospheric events is 10 minutes; this conclusion remains the same for every cut-off

angle analyzed in table 5. However, we can observe that there is still a relation between the number of events and the cut-off angle: we detect more ionospheric events when the cut-off angle is low. This conclusion is the same as the one for DOY 324/03, which is logical.

This obvious independency between number of events and time interval is due to the fact that a TID has its own period and wavelength. For example, if we consider a time interval corresponding to a quarter (or a half) of this wavelength, variance of the residual is inevitably lower than the variance obtained with a time interval corresponding to the full wavelength. Therefore, by looking at table 5, we could say that the period of the TID which happened on DOY 359/04 had probably a period of about 10 minutes. However, let us recall that the number of events shown in table 5 is the sum of all events detected during this day and that other ionospheric phenomena could also influence this total number of events.

		Time interval [min]					
		5	**10**	**15**	**20**	**30**	**r^2**
Cut-off angle [°]	**10**	55	116	91	79	58	0.074548
	15	31	84	69	58	48	0.000166
	20	17	53	44	39	33	0.017753
	25	9	35	32	26	23	0.047627
	30	6	27	25	20	19	0.086834

Table 5. Number of ionospheric events detected for the DOY 359/04 (TID of moderate amplitude) for different time intervals and different cut-off angles

While considering the analysis of a day where a TID occurred, we can say that the use of a time interval different from 15 min may change the temporal distribution of the irregularities which was presented in section 4.1. To verify this hypothesis, we compute the sum of all ionospheric events detected in every time interval by considering the whole years 2001 for solar maximum and 2006 for solar minimum (as in section 4.1). The time interval has been fixed at 10min, 15min (reference time interval) and 20min; the results are shown in figures 4.13 & 4.14.

The analysis of figures 4.13 & 4.14 shows that the absolute values of the number of detected events depend on the time interval: the larger is the time interval, the larger is the number of detected events. Thereby, these values cannot be taken into account to compare the different distributions. Nevertheless, when comparing the shapes of the distributions of the events in function of local time, we can say that they are similar. In conclusions, the time interval does not influence the final conclusions of the section 4.1.

The choice of a time interval of 15min has been made because positioning errors appearing in WP230 are computed every 15min; therefore the number of ionospheric events detected within these time intervals may be a good indicator on the source of the positioning error.

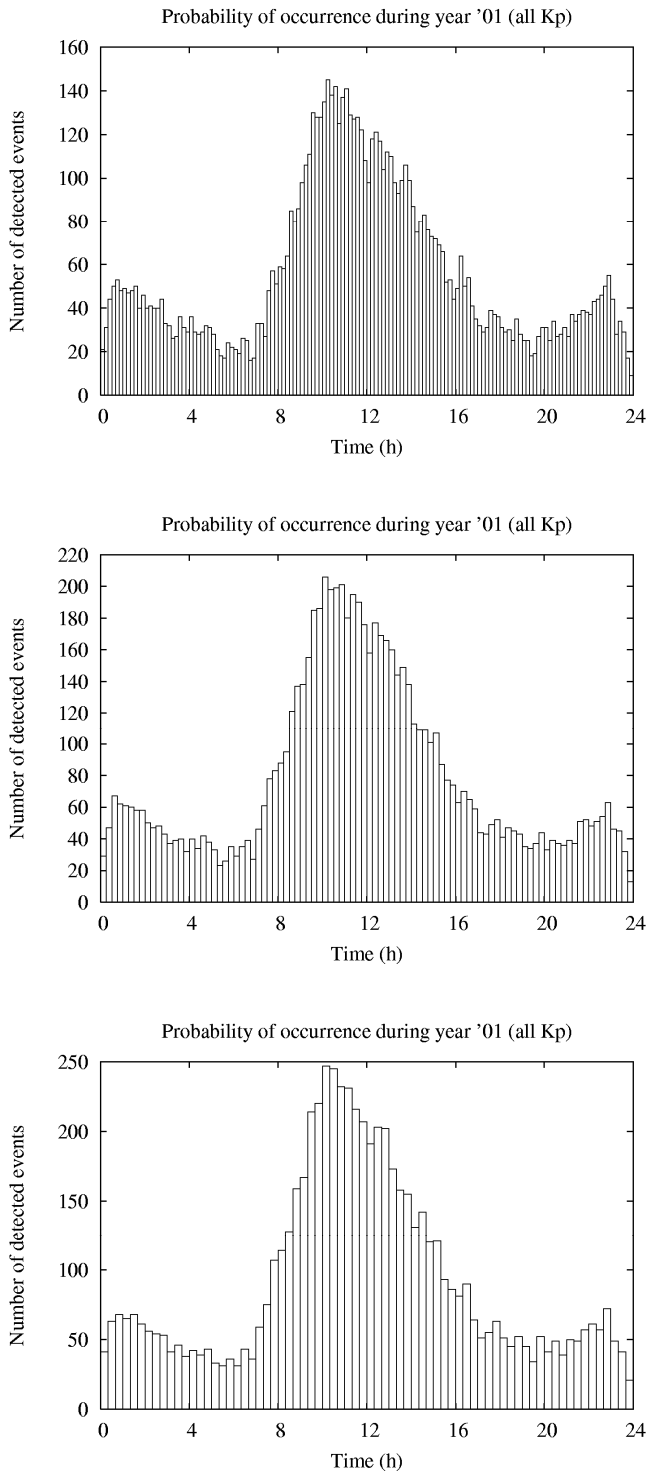

Figure 4.13 Number of ionospheric events detected at Brussels in 2001 in function of local time for time intervals of 10min (top), 15min (middle) and 20min (bottom).

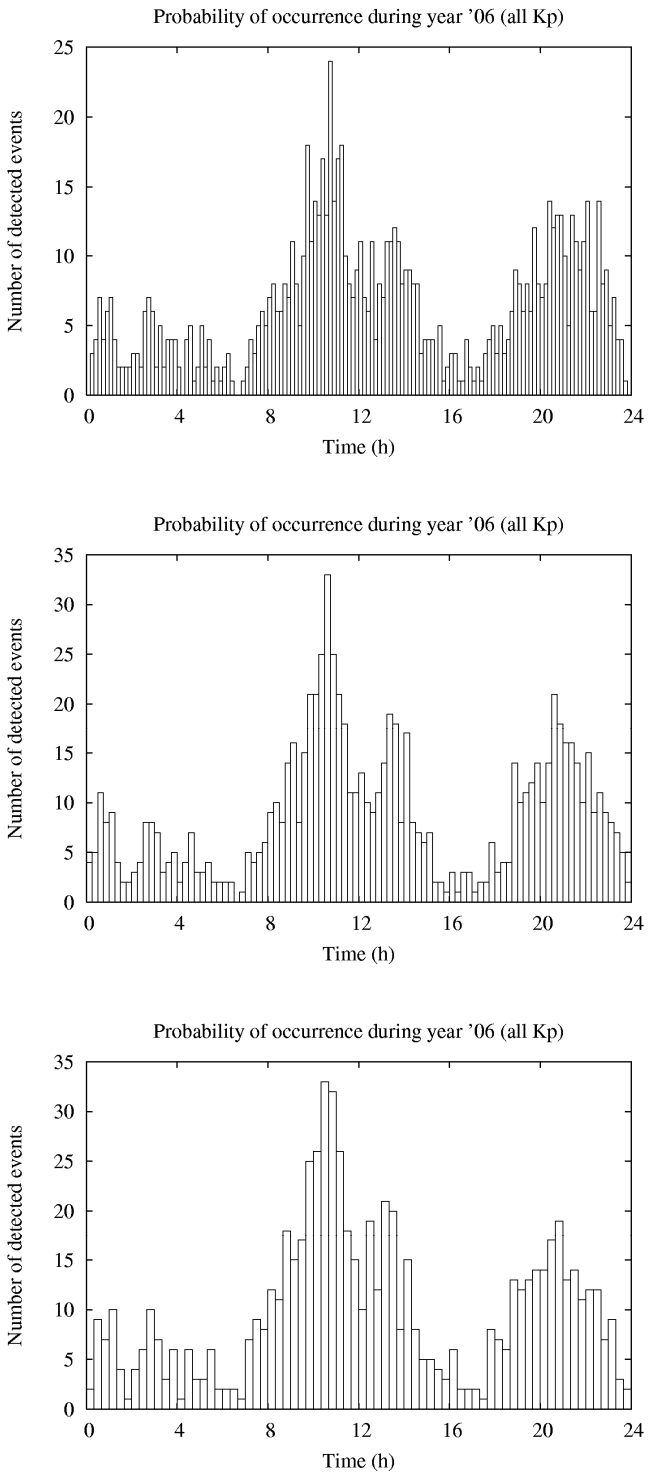

Figure 4.14 Number of ionospheric events detected at Brussels in 2006 in function of local time for time intervals of 10min (top), 15min (middle) and 20min (bottom).

5. GRADIENTS IN SPACE DUE TO IONOSPHERIC SMALL-SCALE DISTURBANCES

The single station method described in paragraph 2 detects small-scale ionospheric disturbances by monitoring RoTEC. Nevertheless, the influence of small-scale disturbances on GNSS differential applications depends on TEC gradients in space between the reference station and the user: this information is not directly supplied by the above-mentioned method.

In practice, to assess the influence of small-scale ionospheric disturbances on differential positioning, we proceed in 2 steps: first, we detect periods with increased ionospheric variability with the single station method. Then, we analyse the gradients in space due to these ionospheric disturbances using the Belgian Active Geodetic Network also called the Belgian Dense Network (BDN).

5.1. The Belgian Active Geodetic Network

Belgium is equipped with an Active Geodetic Network (AGN) of 61 reference GPS stations (Figure 5.1). The role of this network is to serve as reference for GNSS real time positioning applications in Belgium. AGN is composed of 3 sub-networks:

- WALCORS: WALlonia Continuous Operating System is a GPS reference network based on 23 stations. This network has been set up by the Topography and Cartography department of the Walloon Region.
- FLEPOS: Flemish Positioning Service is a public service based on 37 permanent reference stations operated and maintained by the Support Centre for GIS of the Flemish government.
- GPSBru: when it will be operational, GPSBrussels will be a network of 3 stations operated for the Region of Brussels by the National Geographic Institute. At the present time, only one station is available.

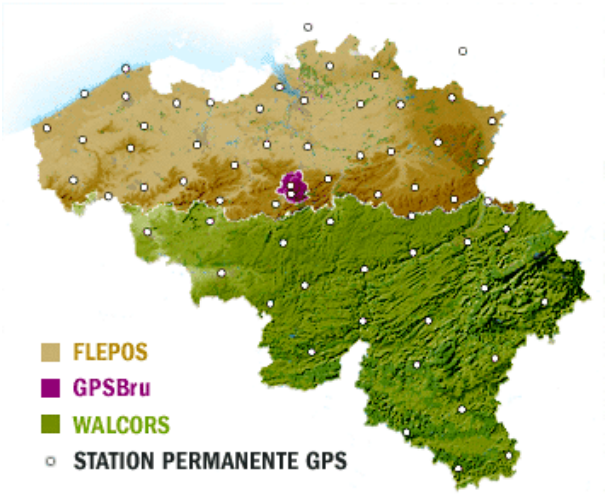

Figure 5.1 The Belgian Active Geodetic Network.

This network is one of the densest permanent networks in Europe: baseline lengths range between 4 km and about 30 km. This high density of stations allows performing a detailed analysis of local TEC gradients in space over Belgium. We shall refer to it as the Belgian Dense Network or BDN.

5.2. Selection of days : case study

The study of the effects of ionospheric structures on double differences has been done through some case studies representing typical disturbed conditions: TID of medium and large amplitude and geomagnetic storm. The choice of the analyzed days is explained below:

- First, we have to select the stations which will be processed. These stations must be chosen in order to answer two fundamental questions about the effects in space of the ionospheric structures (see section 5.5.1):

  1) Has the length of the baseline an influence on the residual ionospheric term in the double differences?
  2) Has the orientation of the baseline an influence on the residual ionospheric term in the double differences?

  If we want to study each question in details, we need to isolate each parameter separately: for this reason, we have to choose different baselines having

  1) the same orientation but significantly different lengths;
  2) the same length and different orientation.

  The geometry of the BDN (figure 5.1) allows then many combinations of stations to fulfil these two conditions.

- Secondly, the selection of the disturbed days is based on the results obtained by the one-station method (see section 2.1). Unfortunately, FLEPOS and WALCORS were not put into service at the same time (October 2002 for FLEPOS and November 2003 for WALCORS) so that the oldest data are only available for the FLEPOS stations. In addition, only a limited number of stations/days from these networks are available at RMI. Therefore, the challenge is to make sure that the stations we want to process were operating during the selected disturbed days.

- Thirdly, we have to check the integrity of the RINEX files and the absence of gaps in these files to avoid problems during the data processing and analysis.

In practice, we have selected 7 stations of the FLEPOS network and formed 5 different baselines (figure 5.2):

- GILL–LEEU (11.3 km) and GILL–MECH (20.5 km) were chosen to study the influence of the baseline length: these lengths present a ratio 1:2 for a similar orientation.
- OUDE–GERA (19.9 km), OUDE–ZWEV (19.4 km) and OUDE–GENT (18.7 km) are the baselines chosen to analyse the effect of the baseline orientation. The lengths are quite similar while the orientations are significantly different from each other.

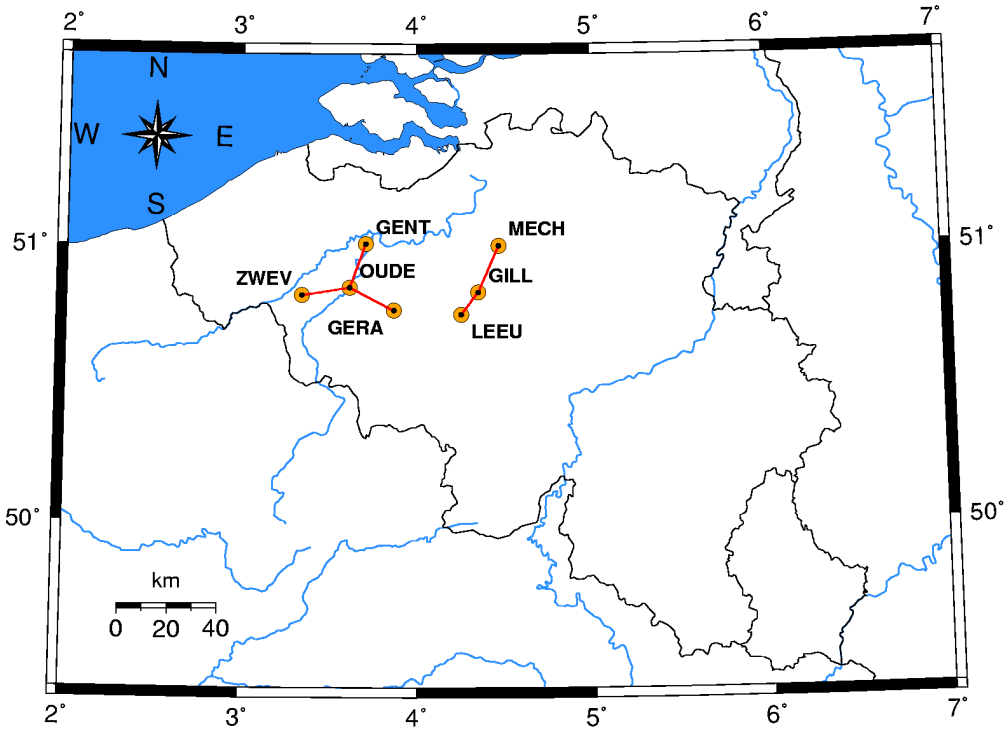

Figure 5.2 Selected baselines.

Furthermore, as every minute of the selected days is not especially disturbed, we have to isolate a small time interval during which the ionospheric structure (TID or noise like structure) clearly occurs. Typically, we have chosen time intervals of 15 minutes within which the variability due to the ionospheric phenomenon was the largest. Let us note that later (see section 5.5.2) we can also extract more than 15 minutes from one day to obtain more results. We based this selection on the results coming from the one-station method which computes the ionospheric variability at the station of Brussels (BRUS); the figures 5.3 to 5.6 show one of the outputs from this one-station software. These files contain the intensity of the ionospheric events (defined in section 2.1) as function of the satellite PRN number (rows) and of GPS time expressed in hours (columns) for the selected days of interest. The ionospheric variability ranges from 0 (marked as a dot) to 9 and is computed every 15 minute time interval; so there are 4 values of the variability per hour.

Thanks to these data, we chose to isolate three disturbed periods which will be studied in details in the next section:

- Day with medium-amplitude TID: 359/04, satellite pair 5/6 (9.725h – 9.966h) ;
- Day with large-amplitude TID: 301/03, satellite pair 7/5 (11.33h – 11.575h) ;
- Day with severe geomagnetic storm: 324/03, satellite pair 16/2 (17.358h – 17.608h).

Moreover, in comparison to disturbed days, we also need to analyse a quiet day in terms of ionospheric variability. This quiet day has been selected based on the following criteria:

- Number of ionospheric events detected by our one-station method as low as possible;
- Planetary index Kp as low as possible (source: NOAA);
- Ionization due to X-rays as low as possible (source: GOES satellite).

We decided to choose the DOY 103/07 because:

- Number of detected ionospheric events at BRUS (Brussels) = 0, as it appears in figure 5.6;
- Daily maximum Kp value = 0.7 ;
- GOES X-rays: Intensity (1-8 Å) < 10^{-8} W/m² → less than A-class.

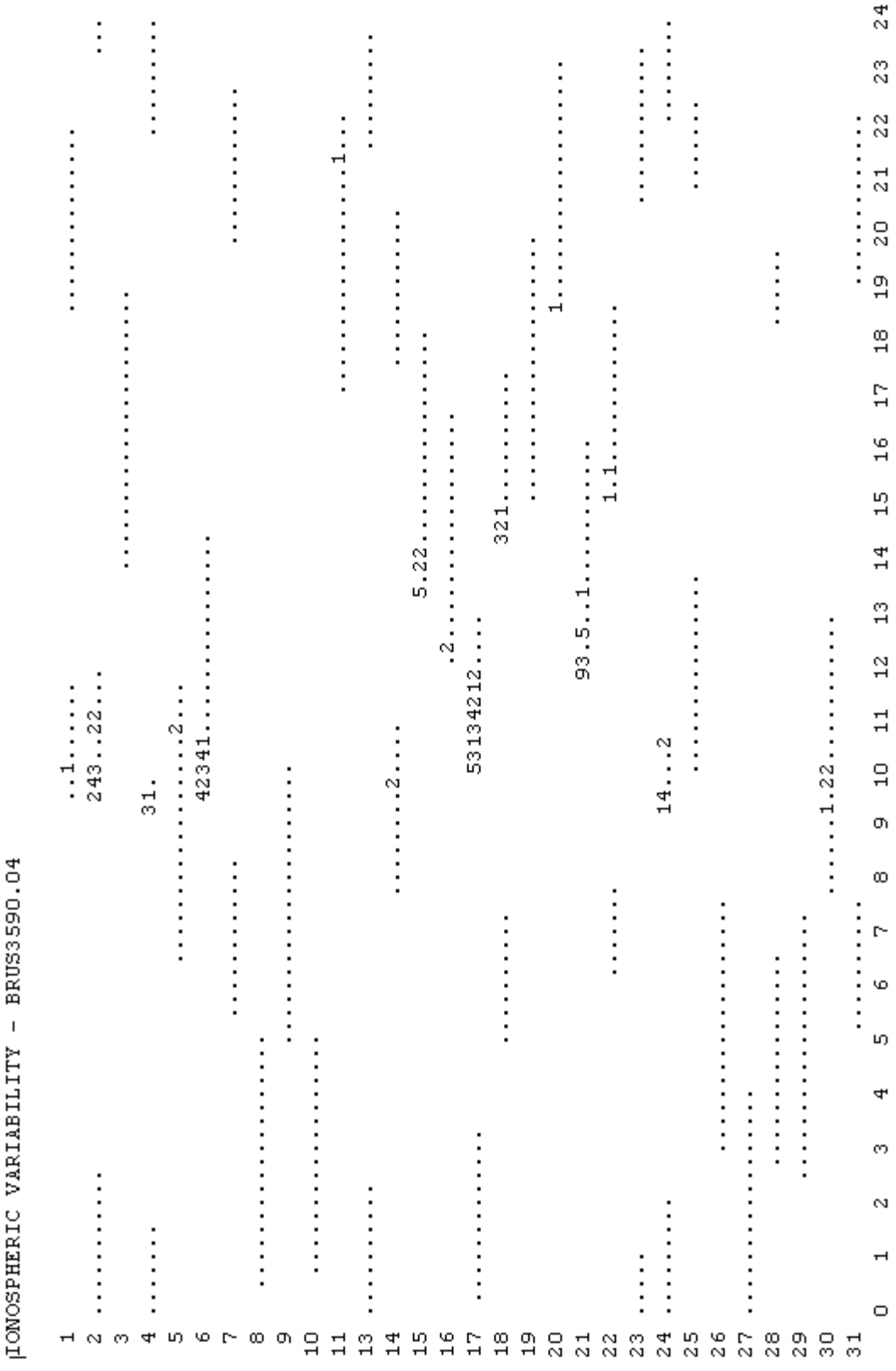

Figure 5.3. Ionospheric variability at station BRUS on DOY 359/04.

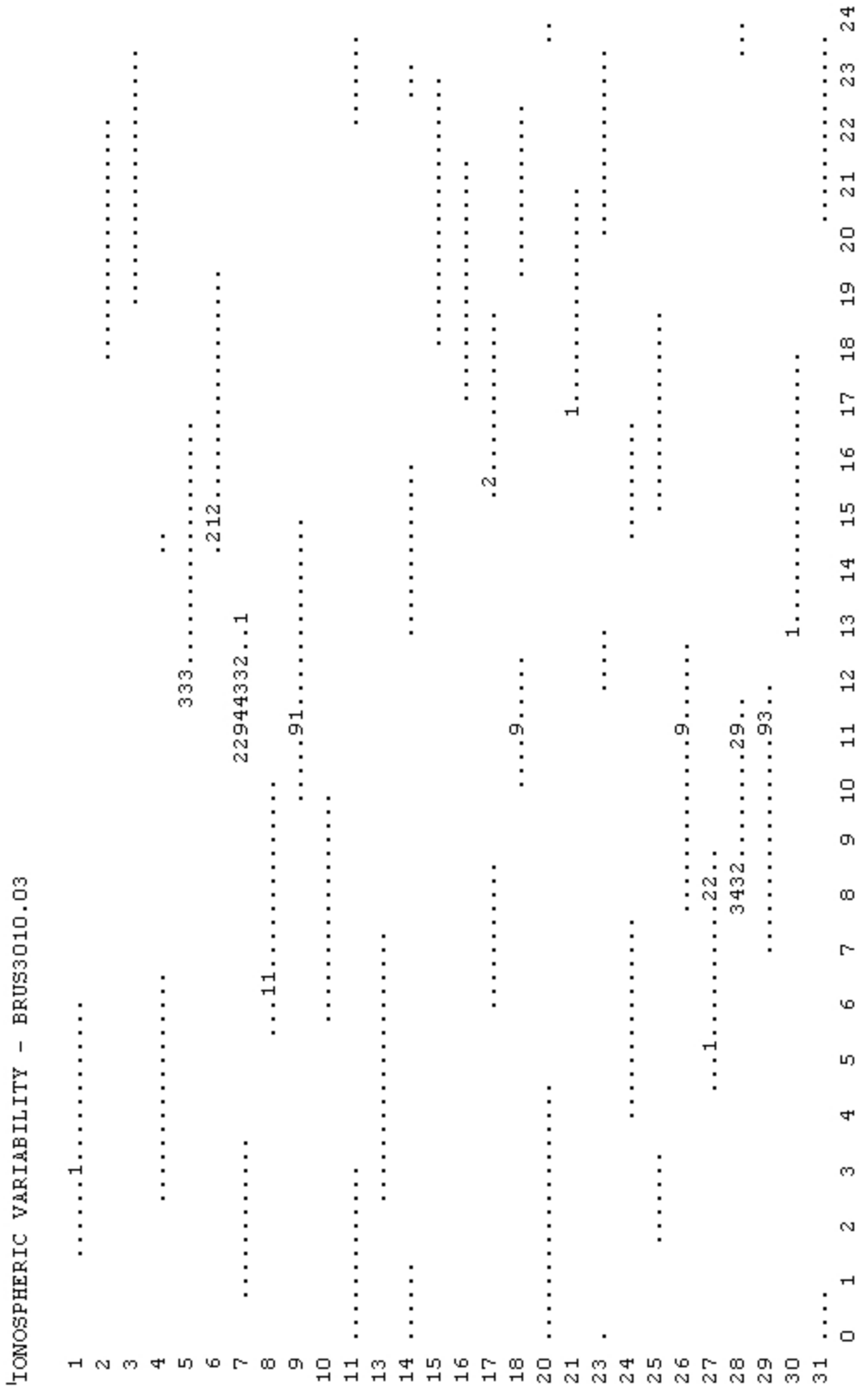

Figure 5.4. Ionospheric variability at station BRUS on DOY 301/03.

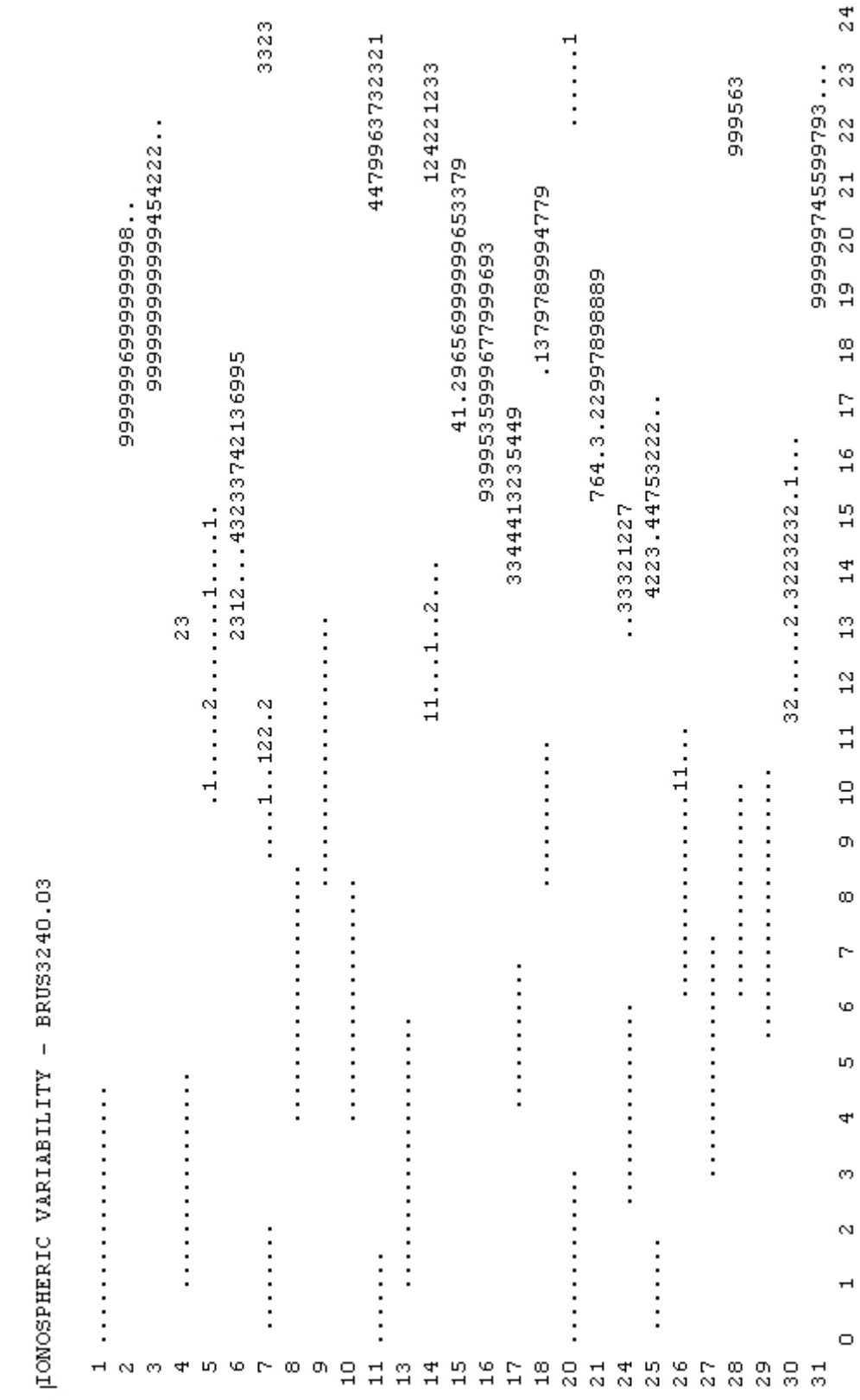

Figure 5.5. Ionospheric variability at station BRUS on DOY 324/03.

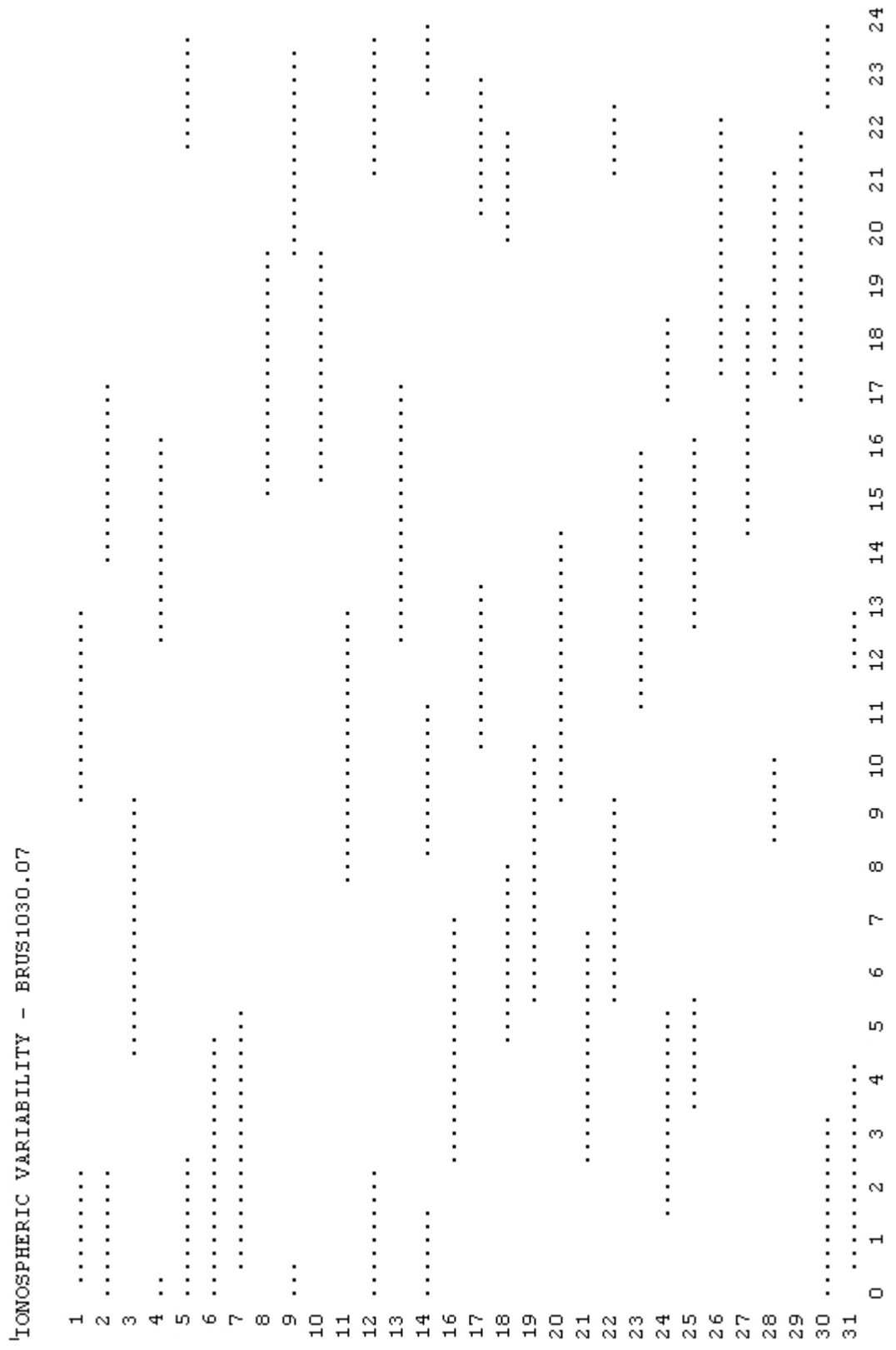

Figure 5.6. Ionospheric variability at station BRUS on DOY 103/07.

5.3. Gradient detection using double differences : methodology

By forming double differences of phase observations collected in the BDN stations of which the positions are precisely known, it is possible to monitor residual differential errors due to small-scale ionospheric disturbances.

The RTK technique can be run both in differential and in relative mode. In differential mode, RTK users receive so-called differential corrections from a reference station. These differential corrections are used to correct the user measurements for errors which are common with the reference station. In relative mode, RTK users combine their own phase measurements with the measurements made by a reference station of which the position is precisely known. In practice, the mobile user forms double differences between its own phase measurements and the phase measurements collected in the reference station. In this report, we call receiver A, the reference station receiver, and receiver B, the user receiver.

If $\varphi^i_{A,k}$ and $\varphi^i_{B,k}$ are phase measurements made simultaneously by receivers A and B on satellite i, the single difference $\varphi^i_{AB,k}$ (k = L1 or L2) is defined as:

$$\varphi^i_{AB,k} = \varphi^i_{A,k} - \varphi^i_{B,k} \tag{5.1}$$

If receivers A and B observe a second common satellite j, we can form a second single difference $\varphi^j_{AB,k}$. Then, the double difference $\varphi^{ij}_{AB,k}$ is defined as:

$$\varphi^{ij}_{AB,k} = \varphi^i_{AB,k} - \varphi^j_{AB,k} \tag{5.2}$$

Based on equation (2.1), equation (5.2) can be rewritten:

$$\varphi^{ij}_{AB,k} = \frac{f_k}{c}\left(D^{ij}_{AB} + T^{ij}_{AB} - I^{ij}_{AB,k} + M^{ij}_{AB,k}\right) + N^{ij}_{AB,k} + \varepsilon^{ij}_{AB,k} \tag{5.3}$$

with the notation :

$$*^{ij}_{AB,k} = (*^i_{A,k} - *^i_{B,k}) - (*^j_{A,k} - *^j_{B,k}) \tag{5.4}$$

In double differences, all the error sources which are common to the phase measurements performed by receivers A and B cancel, in particular, satellite and receiver clock errors. In addition, in the case of RTK, which is used on short distances, orbit residual errors can be neglected (Seeber, 2003). Residuals atmospheric effects T^{ij}_{AB} and $I^{ij}_{AB,k}$ depend on the distance between A and B and also on the atmospheric "activity". Given the short distances considered, RTK data processing algorithms assume that residual atmospheric errors are negligible. In this case, neglecting multipath and noise, equation (5.3) can be rewritten:

$$\varphi_{AB,k}^{ij} = \frac{f_k}{c} D_{AB}^{ij} + N_{AB,k}^{ij} \tag{5.5}$$

In the case of the BDN, both station A and B positions are known. Therefore, using ephemeris data, the distance term D_{AB}^{ij} can be computed. Then, from equation (5.5), it comes:

$$\varphi_{AB,k}^{ij} - \frac{f_k}{c} D_{AB}^{ij} = N_{AB,k}^{ij} \tag{5.6}$$

In other words, if equation (5.5) is valid (i.e. if the residual errors remain negligible), the L1 or L2 double difference corrected for the distance term should remain close to an integer constant. When small-scale ionospheric disturbances are present, they produce residual effects which are visible in the double differences of L1 or L2 phase measurements. As an illustration, figure 5.2 shows double differences of L1 made with the data collected in the stations Brussels and Saint-Gilles (4 km baseline) on December 24 2004 for 2 satellite pairs. These double differences are corrected for geometric terms (station and satellite positions) according to equation (5.6). In other words, these double differences only contain the ambiguity term (which is an integer number) and non-modelled residual errors which are usually very small on a 4 km baseline; this is the case in figure 5.2 (left) for satellite pair 28-27 where the double differences remain very close to the integer value of the ambiguity what means that residual errors are negligible. Double differences on satellite pair 21-6 show a very different behaviour (Figure 5.2, right): a TID, which has been detected on both satellite 21 and 6 using the single station method, is the origin of peak to peak variability of about 0.6 L1 cycles (11.5 cm) even on a short baseline of 4 km.

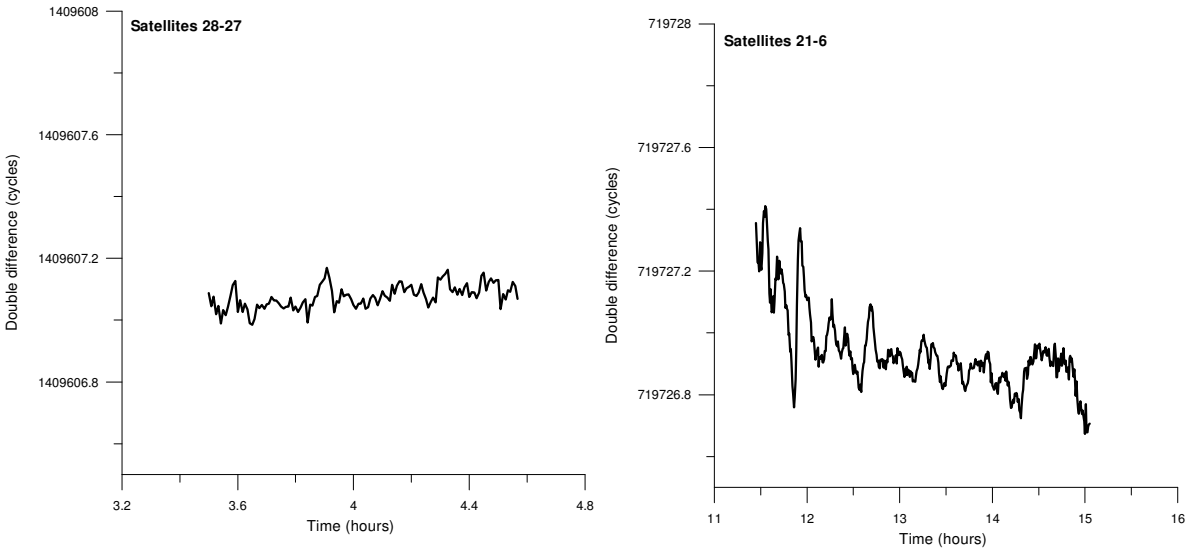

Figure 5.2 Double difference of the L1 phase (in L1 cycles) on DOY 359 in 2004, baseline Brussels-Saint Gilles (4 km), satellite pair 28-27 (left) and satellite pair 21-6 (right).

When residual effects are present in double differences of L1 or L2, they could be due to other sources than the ionosphere. Therefore, to detect residual effects which are due to the ionosphere, we use the geometric-free combination $\varphi^{i}_{A,GF}$.
The geometric free combination is given by (equation 2.4):

$$\varphi^{i}_{A,GF} = 0,552\ 10^{-16}\, TEC^{i}_{A} + M^{i}_{A,GF} + N^{i}_{A,GF} + \varepsilon^{i}_{A,GF} \tag{5.7}$$

Let's recall that this combination is called "geometric free" due to the fact that it does not contain geometric terms (i.e. satellite and receiver coordinates). Therefore, it cannot be used to compute the user position. Using the notation defined in equation (5.4), the double difference of the geometric free combination is given by:

$$\varphi^{ij}_{AB,GF} = 0,552\ 10^{-16}\, TEC^{ij}_{AB} + M^{ij}_{AB,GF} + N^{ij}_{AB,GF} + \varepsilon^{ij}_{AB,GF} \tag{5.8}$$

This equation can be rewritten as:

$$\varphi^{ij}_{AB,GF} - N^{ij}_{AB,GF} = 0,552\ 10^{-16}\, TEC^{ij}_{AB} + M^{ij}_{AB,GF} + \varepsilon^{ij}_{AB,GF} \tag{5.9}$$

If we neglect noise and multipath:

$$\varphi^{ij}_{AB,GF} - N^{ij}_{AB,GF} = 0,552\ 10^{-16}\, TEC^{ij}_{AB} \tag{5.10}$$

In other words, the differential ionospheric effect (i.e. differential TEC) can be obtained by forming double differences of the geometric free combination. This is the strategy we have used. In the next paragraphs we will rename this term $I^{ij}_{AB,GF}$ so that

$$I^{ij}_{AB,GF} = 0.552\ 10^{-16} TEC^{ij}_{AB} \tag{5.11}$$

Let us remark that in equation (5.10) the ambiguity $N^{ij}_{AB,GF}$ has been computed by using the whole time series of the satellite pair considered. In other words, this ambiguity $N^{ij}_{AB,GF}$ is not a "real-time" ambiguity because its resolution requires the knowledge of all available phase measurements for the considered satellite couple. To solve the integer ambiguities $N^{ij}_{AB,L1}$ and $N^{ij}_{AB,L2}$, the calculation implemented in our software uses the resolution of the wide-lane ambiguity ($N^{ij}_{AB,WL}$) which could be solved (*i.e.* fixed at its correct integer value) nearly all the time thanks to its large wavelength of about 86cm:

$$N^{ij}_{AB,WL} = N^{ij}_{AB,L1} - N^{ij}_{AB,L2} \tag{5.12}$$

5.4. Quantitative analysis of ionospheric residual effects

5.4.1. Overview of the case studies in double differences

In order to illustrate the different cases studied in the following sections, we plot the double difference phase measurements as described by the equation (5.6), *i.e.* the double differences corrected with the geometry term for each of theses cases (figure 5.3). We have computed several baselines but we show in figure 5.3 only the data relative to the baseline OUDE-ZWEV (19.4 km), as an illustration.

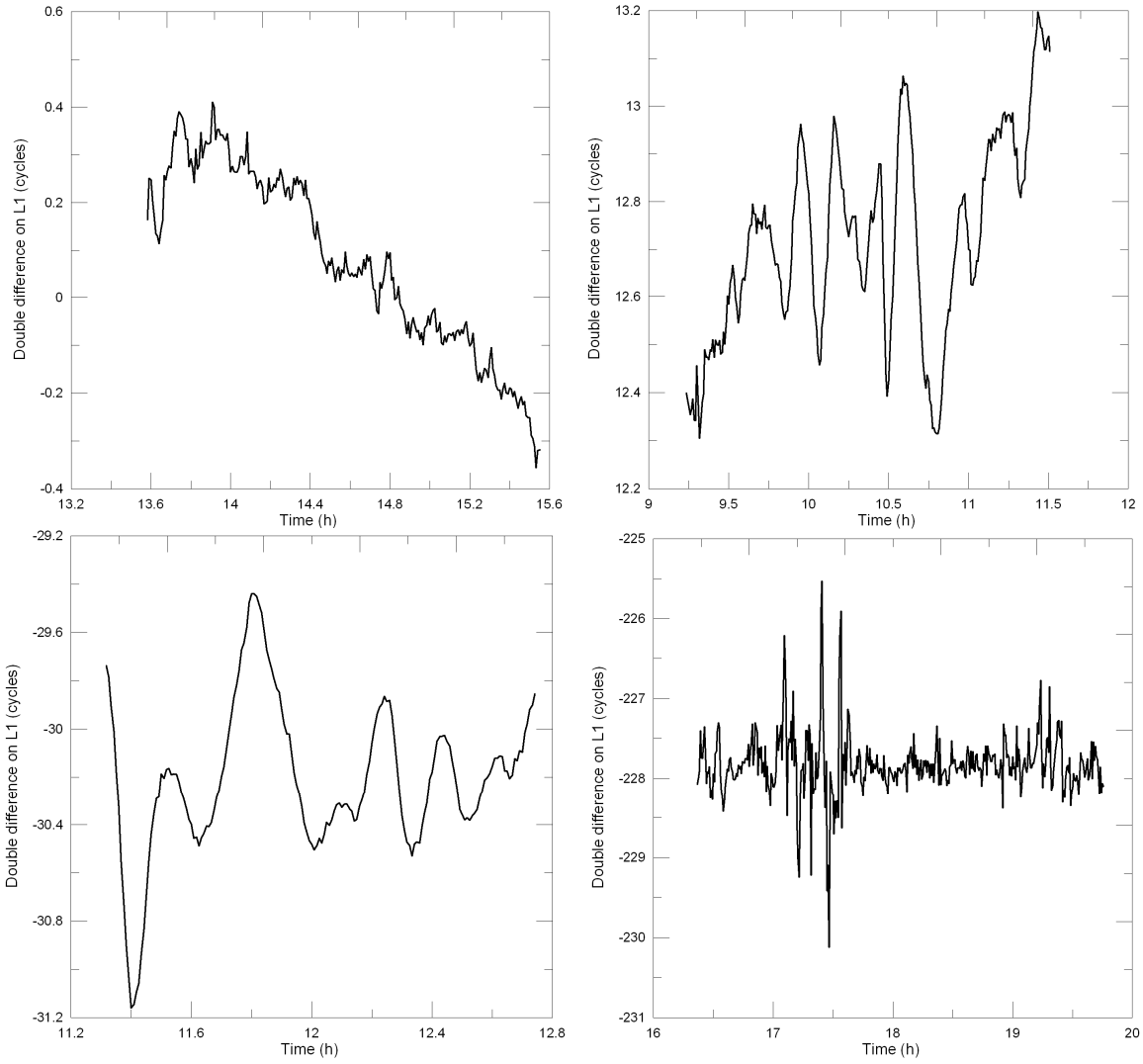

Figure 5.3 Double differences of the L1 carrier for the baseline OUDE-ZWEV, on DOY 103/07 satellite pair 23/2 (top left), DOY 359/04 satellite pair 5/6 (top right), DOY 301/03 satellite pair 7/5 (bottom left) and DOY 324/03 satellite pair 16/2 (bottom right).

When analyzing these plots, we can observe that the ionospheric structures can induce very different effects on the double differences (scales are different on the 4 plots) and that the peak-to-peak variability can reach more than 4 cycles in a few minutes in the case of a geomagnetic storm (DOY 324/03).

5.4.2. Quantitative analysis

In this section, we will present some statistics about the residual ionospheric term $I^{ij}_{AB,GF}$ computed by using the equation (5.10) for the five different baselines described in section 5.2. This study will assess the differential effect of the ionosphere during several cases of disturbed conditions.

The main statistics we formed are the mean of the absolute values and the standard deviation of $I^{ij}_{AB,GF}$ within a quarter of hour. Moreover, the mean has been normalized with respect to the length of the baseline, so that the values relative to different baselines are made comparable with each other. The sampling rate is 30 s, what means that we have 30 observations for each 15 minute time interval. The values of the mean and of the standard deviation, expressed in length units (meters or millimeters) and in TEC units (TECU) according to equation (5.11), are shown in tables 6 to 10.

	Average		**Std Deviation**		**Normalized Average**	
	[mm]	[TECU]	[mm]	[TECU]	[mm/km]	[TECU/km]
103/07	3.3	0.031	3.1	0.029	0.29	0.003
359/04	19.0	0.181	19.1	0.182	1.68	0.016
301/03	48.9	0.466	39.9	0.380	4.33	0.041
324/03	65.1	0.620	85.2	0.811	5.76	0.055

Table 6. Statistics of $I^{ij}_{AB,GF}$ for the baseline GILL - LEEU (11.3 km).

	Average		**Std Deviation**		**Normalized Average**	
	[mm]	[TECU]	[mm]	[TECU]	[mm/km]	[TECU/km]
103/07	3.3	0.031	4.2	0.040	0.16	0.002
359/04	38.9	0.370	38.6	0.368	1.90	0.018
301/03	61.6	0.586	76.3	0.726	3.00	0.029
324/03	142.4	1.356	196.0	1.865	6.95	0.066

Table 7. Statistics of $I^{ij}_{AB,GF}$ for the baseline GILL - MECH (20.5 km).

	Average		Std Deviation		Normalized Average	
	[mm]	[TECU]	[mm]	[TECU]	[mm/km]	[TECU/km]
103/07	3.2	0.030	3.5	0.034	0.16	0.002
359/04	17.4	0.166	19.8	0.188	0.87	0.008
301/03	87.0	0.828	87.3	0.831	4.37	0.042
324/03	59.3	0.565	81.2	0.773	2.98	0.028

Table 8. Statistics of $I^{ij}_{AB,GF}$ for the baseline OUDE - GERA (19.9 km).

	Average		Std Deviation		Normalized Average	
	[mm]	[TECU]	[mm]	[TECU]	[mm/km]	[TECU/km]
103/07	5.1	0.049	4.5	0.043	0.26	0.003
359/04	16.3	0.155	16.0	0.152	0.84	0.008
301/03	49.1	0.467	55.2	0.526	2.53	0.024
324/03	88.5	0.842	119.9	1.141	4.56	0.043

Table 9. Statistics of $I^{ij}_{AB,GF}$ for the baseline OUDE - ZWEV (19.4 km).

	Average		Std Deviation		Normalized Average	
	[mm]	[TECU]	[mm]	[TECU]	[mm/km]	[TECU/km]
103/07	3.1	0.030	4.0	0.038	0.17	0.002
359/04	36.3	0.346	40.4	0.385	1.94	0.018
301/03	52.9	0.504	55.4	0.528	2.83	0.027
324/03	158.6	1.510	173.0	1.647	8.48	0.081

Table 10. Statistics of $I^{ij}_{AB,GF}$ for the baseline OUDE - GENT (18.7 km).

From tables 6 to 10 we can observe that geomagnetic storms are the phenomena which induce the largest ionospheric residual error; this is due to the strong temporal gradients of the TEC that we have observed with our one-station method (see section 4.2.2).

The analysis of tables 6 to 10 shows also that for all the baselines the ionospheric term remains very close to a single value during the quiet day 103/07: about a 3 mm of average for a standard deviation of 3-4 mm. Let us remark that this value is of the same order of magnitude than the measurement noise on double differences of the geometric free combination (which is about 3.5 times the noise of the L1 carrier).

We can also see that for a given day the effect of the ionospheric structure can be very different from a baseline to another. For example, we can observe that the mean value of $I^{ij}_{AB,GF}$ during the 15 minute period of DOY 359/04 is smaller for a baseline of about 20

km (OUDE-GERA) than for a baseline of 11 km (GILL-LEEU). Another example is given when considering the standard deviation during DOY 324/03 for the baselines GILL-MECH and OUDE-GERA: for a similar baseline length, the variability is more than 2 times larger for the first one. Therefore, it is difficult to give an order of magnitude of the residual ionospheric effect on the double differences because it fluctuates very strongly depending on baseline orientation. However, we can give the maximum and the minimum value of the normalized average observed in the five baselines for each of the analyzed days (see table 11).

	Normalized average min		**Normalized average max**	
	[mm/km]	[TECU/km]	[mm/km]	[TECU/km]
103/07	0.16	0.0015	0.29	0.0028
359/04	0.84	0.0080	1.94	0.0185
301/03	2.53	0.0241	4.37	0.0416
324/03	2.98	0.0284	8.48	0.0807

Table 11. Minimum and maximum values of the normalized average observed in the five baselines.

Moreover, we can see that the variability (*i.e.* the standard deviation) is nearly twice larger for a 20 km baseline (GILL-MECH) than for a 11 km one (GILL-LEEU). This difference between these two baselines having the same orientation is much more visible through the standard deviation that through the mean values. This observation allows us to expect that the influence of the baseline length is not negligible: this is the reason why this effect will be analyzed in more details through a statistical method explained in the next section.

Finally, the significantly different values of the mean and of the standard deviation for similar baseline lengths allow us to think that the orientation of the baseline plays certainly a role in the way that the structure is "seen" through the double differences. This point is also discussed in more details in the next section.

5.5. Influence of the length and the orientation of the baseline

5.5.1. Methodology

In the previous sections, we have seen that for a similar baseline orientation, the distance between the two stations influenced the order of magnitude of the residual ionospheric term $I^{ij}_{AB,GF}$. Therefore, we can expect that for a longer baseline, the atmospheric residual errors in double differences will be larger. On this basis, the strategy to use is to prove that the ionospheric residual error is larger for a long baseline than for a smaller one by using another method than simply comparing the values in the tables.

In the case of a TID, we can expect that the baseline orientation plays an important role in the distribution of the ionospheric residual error. Indeed, let us consider a planar wave propagating southwards. On one hand, we can deduce that a baseline which is exactly oriented along the direction West-East will observe a very weak ionospheric residual term because the vector linking the two stations is parallel to the front wave (which is of course perpendicular to the direction of propagation). On the other hand, a baseline oriented along the direction North-South would observe the largest TEC gradients induced by the TID. The values displayed in the tables in the previous section tend to confirm this statement. In this way, the strategy to use is to prove (or not) that the baseline orientation has an influence on the variability of the ionospheric term $I^{ij}_{AB,GF}$.

The two hypotheses explained above have been tested by using a statistical technique based on a statistical test (hypothesis testing):

- In order to assess the effect of the baseline length, we want to prove that the variability of $I^{ij}_{AB,GF}$ is significantly <u>larger</u> for a baseline of about 20 km (GILL-MECH) than for a baseline of 11 km (GILL-LEEU).

- To analyze the effect of the orientation of the baseline, we have to check if the variability of $I^{ij}_{AB,GF}$ is significantly <u>different</u> from a baseline to another. We will use the three baselines OUDE-GERA, OUDE-ZWEV and OUDE-GENT.

In the two cases, the strategy uses the Fisher's test which is explained below.

> Let us consider two groups G_1 and G_2; and their respective variance V_1 and V_2. We would prove that the variance in G_2 is greater than the variance into the group G_1, so $V_2 > V_1$. The null hypothesis, which can be described as the hypothesis that might be rejected at the end of the statistical test, is logically written as follows:
>
> $$H_0 : V_2 \leq V_1$$
>
> The alternative hypothesis H_1 is written as follows: $H_1 : V_2 > V_1$
>
> Let us now consider that we have two samples of data containing respectively N_1 and N_2 data points, in reference to the groups G_1 and G_2. The estimated variances are called respectively v_1 and v_2.
>
> Then, we have to form the Fisher's test called F:
>
> $$F = \frac{v_2}{v_1} \qquad (5.11)$$

The null hypothesis H_0 is rejected if the Snedecor's test Q_F is smaller than the quantity F for a significance level α. In our work, this significance level is 5% (α = 0.05) and Q_F has (N_1-1) and (N_2-1) degrees of freedom. So, we reject H_0 if:

$$F > Q_F(0.05; N_2 - 1; N_1 - 1)$$

Finally, the alternative hypothesis H_1 is valid if H_0 is rejected; we prove then statistically that $V_2 > V_1$.

The previous explanation was valid to test the effect of the length of the baseline where the hypothesis was that a variance is larger than the other one. However, if we want to prove that the two variances are significantly different from an orientation to another, we have to change a few variables in our test:

- The null hypothesis is the identity of the two variances: $H_0 : V_2 = V_1$
- The alternative hypothesis is the inequality of these variances: $H_1 : V_2 \neq V_1$
- The F test is the same as written in equation (5.11) but with $v_2 > v_1$
- The computation of Q_F is the same as for the previous test and if we reject H_0 we prove that V_1 and V_2 are statistically different from each other (i.e. $V_2 \neq V_1$).

5.5.2. Effect of the length

In section 5.4.2 we have seen that the length of the baseline has an influence on the value of the residual ionospheric term; this analysis was based on a time interval of 15 minutes. In the present analysis, the comparison of the two baselines GILL-LEEU (11.3 km) and GILL-MECH (20.5 km) can be made on the basis of several time intervals within the same disturbed period of the selected days. We chose 3 periods of 15 minutes for each day and we consider also the whole visibility period of the satellite pair. Let us recall that as the observation rate is 30 s, each 15 minute period contains 30 observations.
For example, the DOY 359/04 has been analyzed when considering 3 intervals of 15 minutes each and the whole visibility period:

09.725h → 09.966h
09.975h → 10.216h
10.225h → 10.466h } the 3 periods of 15 minutes each
09.225h → 11.483h ⟶ whole visibility period of the satellite pair

In this way, we obtain 4 values of the variance for each disturbed day. Moreover, we also take into account the DOY 103/07 (quiet in terms of ionospheric activity) so that we can assess the effects of the quiet ionosphere on the residual term in double differences too. However, especially for this day, we take only one 15 minute period at random.

Finally, we have 13 variance values for each of the two baselines and we apply the Fisher's test to all of these variances; the results are shown in table 12.

	103/07	**359/04**			
	14.1h-14.3h	9.7h-9.9h	9.9h-10.2h	10.2h-10.4h	9.2h-11.5h
F	1.8889	4.0765	2.5055	5.0355	4.1814
QF	0.5374	0.5374	0.5374	0.5374	0.8187

	301/03			
	11.3h-11.5h	11.5h-11.8h	11.8h-12.1h	11.3h-12.8h
F	3.6470	3.9264	2.5763	3.5163
QF	0.5374	0.5374	0.5374	0.7782

	324/03			
	17.1h-17.3h	17.3h-17.6h	17.6h-17.8h	16.3h-19.7h
F	3.4986	5.2901	1.7517	4.3730
QF	0.5374	0.5374	0.5374	0.8493

Table 12. Fisher's test during the different periods for the assessment of the effect of the length of the baseline.

If we count the number of times that $F > Q_F$ we can say that for all of these cases the null hypothesis H_0 has to be rejected, and so that the variance for the baseline GILL-MECH is significantly larger than the variance for the baseline GILL-LEEU in 100% of the studied cases.

These results mean that the length of the baseline has a significant influence on the residual ionospheric term in double differences, even during quiet ionospheric periods. If the length of the baseline increases, the variability of the residual ionospheric term increases too.

5.5.3. Effect of the orientation

Here, we analyze the effect of the baseline orientation on the variability of $I^{ij}_{AB,GF}$. We use the same time intervals as in section 5.5.2, what means that there will be 13 values of variance for each baseline.

The baselines selected for this study are OUDE-GERA (19.9 km), OUDE-ZWEV (19.4 km) and OUDE-GENT (18.7 km) which are shown in figure 5.2.

Following the Fisher's test to detect the inequality of variances, we have to make 3 different tests corresponding to 3 different null hypotheses:

1. $H_0 : V_{OUDE-GERA} = V_{OUDE-ZWEV}$
2. $H_0 : V_{OUDE-GERA} = V_{OUDE-GENT}$
3. $H_0 : V_{OUDE-GENT} = V_{OUDE-ZWEV}$

In this way, we obtain 3 times 13 values of Fisher's test. The results will not be shown into tables because of the amount of data but we show the counts of the number of times that we rejected the null hypothesis (table 13).

	number of counts F > QF (H0 rejected)
OUDE-GERA VS OUDE-ZWEV	13
OUDE-GERA VS OUDE-GENT	13
OUDE-GENT VS OUDE-ZWEV	13

Table 13. Results of Fisher's test for the assessment of the effect of the orientation of the baseline.

These statistical results show that every baseline orientation induces its own ionospheric residual variability in comparison with the other ones, as we have already observed in the values shown in tables 6 to 10. Therefore, we can conclude that the orientation plays an important role in the way that double differences "perceive" the ionospheric structures, as expected.

5.6. Determination of "ionospheric disturbed conditions"

The one-station method developed in section 2.1 allows to detect the ionospheric temporal variability from the phase measurements made at one station. Nevertheless, this method does not supply the direct contribution of this variability to the double differences and then does not give any information about the gradients in space due to the ionosphere. Nevertheless, these gradients play a crucial role during the processing of the data by RTK users and could be at the origin of positioning errors.

Therefore, in order to create a service dedicated to RTK users which can determine whether the double differences are disturbed (or not) by the ionosphere, the suggested solution is to define a nominal value of the ionospheric residual error during quiet ionospheric conditions. This typical condition has to be quantified for each baseline belonging to the monitoring network on which the RTK service is based. In the future, this network could include all the 61 GPS stations of the Belgian Dense Network (BDN). Then, we could determine whether a baseline is in « ionospheric disturbed condition » by using a statistical method which compares the residual ionospheric error in real-time with the nominal ionospheric error for this baseline. If it is the case, the service could then declare that the baseline is in « ionospheric disturbed condition », what means that there is a significant threat for high precision applications and that ionospheric conditions can

induce a degradation of the RTK positioning. Finally, warning messages could be sent to users.

The strategy used in this study is to compute the nominal variability in double differences for each of the five studied baselines. Afterwards, we will test whether these baselines present a ionospheric residual term significantly larger than the nominal one.

5.6.1. Evaluating the ionospheric nominal conditions in double differences

For each of our test baselines, we chose to base the quantification of the nominal conditions on the variance of $I^{ij}_{AB,GF}$ during a quiet ionospheric day: DOY 103/07. This variance is computed for each visibility period of the satellite pairs, so that we obtain many different variances for the considered baseline. Then, we have to compute a single value representing the average variability during the whole day: this is done by using the mean value of all variances measured during the day:

$$\sigma^2_{day} = \frac{\sum_{i=1}^{n} \sigma_i^2}{n}$$

with *n* the number of the satellite pairs observed for the baseline during the quiet day.

The nominal conditions for each baseline are presented in table 14:

	Variance [m²]	Std. Deviation [mm]
GILL - LEEU	0.000032	5.47
GILL - MECH	0.000047	6.569
OUDE - GERA	0.000062	7.4
OUDE - ZWEV	0.000054	6.921
OUDE - GENT	0.000057	7.164

Table 14. Nominal values of the variance and the standard deviation for the DOY 103/07 (quiet ionosphere).

5.6.2. Tests on the baselines

In this section, we use the same statistical test as previously to determine whether the baselines present a variability significantly larger during the disturbed days than during the quiet day. This test is the Fisher's test explained in section 5.5.1.

As we would prove that the variability is larger during the disturbed days, the null hypothesis can be written as follows:

$$H_0 : V_{disturbed} \leq V_{quiet}$$

Of course, the alternative hypothesis is:

$$H_1 : V_{disturbed} > V_{quiet}$$

Like in section 5.5.1, we reject H_0 if:

$$F = \frac{v_{disturbed}}{v_{quiet}} > Q_F(0.05; N_2 - 1; N_1 - 1)$$

We also use three 15 minute time intervals and the whole visibility period of the satellite pair to compute these statistics; so there are 4 variances per day. As there are 5 different baselines, we have to test 20 variances per day. Then, we can count the number of times that the null hypothesis (*i.e.* identity of the variances) is rejected; the results are presented in table 15.

	number of counts F > QF (H0 rejected)
Var. 359/04 >? Var. 103/07	20
Var. 301/03 >? Var. 103/07	20
Var. 324/03 >? Var. 103/07	20

Table 15. Results of the Fisher's test on the equality of variances between disturbed and quiet days.

We clearly see that for all the analyzed periods, the ionospheric residual term present a variability significantly larger during disturbed days than during the quiet one. That means that the procedure of the RTK service as described in section 5.6 seems to work on our tested data (days and baselines) and could be implemented in the future

6. CONCLUSIONS

The goal of this report was to characterize small-scale structures in TEC which could pose a threat for high accuracy real time GNSS applications.

In a first step, we outlined a technique called the "one-station method" which detects ionospheric disturbances by monitoring high frequency changes in the geometric free combination of L1 and L2 GPS carriers collected at a single station: as ionospheric disturbances are moving, we can expect that such structures will induce TEC temporal variability which can be detected at a single station. We applied the one-station method to the GPS data collected at the permanent (mid-latitude) station of Brussels from 1994 to

2006. Two main types of structures have been observed: Travelling Ionospheric Disturbances and so-called noise-like structures. We have performed a climatological study of these phenomena on a period which covers one solar cycle. TID's have strong seasonal and solar cycle dependence when noise-like structures are "ionospheric variability" which is usually observed during geomagnetic storms. In addition, we have analyzed the "worst case" events identified during the period of our study: the most powerful solar flare ever observed in EUV on October 28th 2003 and the extreme geomagnetic storm which followed this event on October 30th 2003 where TEC variability reached the level of 9.8 TECU/min.

The one-station method allows to measure variability in time but high accuracy real time GNSS applications are affected by variability in space between the user and the reference station. Therefore, in a second step, we measured TEC differential variability (i.e. TEC variability in space) using double differences of the geometric free combination of phase measurements collected in the Belgian Dense Network. From this study, we can conclude that:

- TEC differential variability depends on baseline length and baseline orientation (with respect to ionospheric disturbance propagation);
- TEC differential variability is significantly larger when the one-station method detects disturbed conditions than during "quiet days" where the one-station method does not detect any disturbances.

Therefore, we can consider that the combination of the one-station method with the double difference method could be used as a tool to send warning to users when degraded positioning conditions are expected. In WP 230, we analyze in more details the relationship which exists between these "indicators" of disturbed ionospheric conditions and the positioning error which affects high accuracy real time GNSS applications.

7. REFERENCES

Hernandez-Pajares M., Juan J. M., Sanz J., 2006, Medium-scale Travelling Ionospheric Disturbances affecting GPS measurements : spatial and temporal analysis, J. of Geoph. Res., Vol. 111, A07S11, doi:1029/2005JA011474.

Leick, A., 2004. GPS Satellite Surveying 3rd Edition. John Wiley & Sons, New York, 435p.

Seeber, G., 2003. Satellite Geodesy Second Edition. de Gruyter, New-York, 589 p.

Wanninger, L., 1992. Monitoring Total Ionospheric Electron Content and Ionospheric Irregularities with GPS. Proc. Of the Symposium on Refraction of Transatmospheric Signals. Den Haag, Netherlands, Geodetic Commission, Publications in Geodesy, No. 36, pp. 141-146.

Wanninger, L., 1994. Der Einfluss der Ionosphaere auf die Positionierung mit GPS. PH.D.Thesis, Wissenschaftliche Arbeiten der Fachrichtung Vermessungswesen der Universität Hannover, Nr. 201, 137 p.(in German).

Warnant, R., 1996. Etude du comportement du Contenu Electronique Total et de ses irrégularités dans une région de latitude moyenne. Applications aux calculs de positions relatives par GPS. Ph.D.Thesis, Série Géophysique (No. Hors-Série) de l'Observatoire Royal de Belgique, Belgium (in French).

Warnant, R., 1998. Detection of irregularities in the TEC using GPS measurements. Application to a mid-latitude station. Acta Geodaetica et Geophysica, Hungarica, vol. 33, pp. 121-128.

Warnant, R., Pottiaux, E., 2000. The increase of the ionospheric activity as measured by GPS. Earth, Planets and Space, vol. 52(11), pp. 1055-1060.

Warnant, R., Kutiev, I., Marinov, P., Bavier, M., Lejeune, S., in press, 2007-1. Ionospheric and geomagnetic conditions during periods of degraded GPS position accuracy : 1. Monitoring variability in TEC which degrades the accuracy of Real Time Kinematic GPS application, Adv. Space Res., Vol. 39, 5, pp. 875-880.

Warnant, R., Kutiev, I., Marinov, P., Bavier, M., Lejeune, S., in press, 2007-2. Ionospheric and geomagnetic conditions during periods of degraded GPS position accuracy : 2. RTK events during disturbed and quiet geomagnetic conditions, Adv. Space Res., Vol. 39, 5, pp. 881-888.